Drosophila CK1-γ, *gilgamesh*, controls PCP-mediated morphogenesis through regulation of vesicle trafficking

William J. Gault, Patricio Olguin, Ursula Weber, and Marek Mlodzik

Department of Developmental and Regenerative Biology, Mount Sinai School of Medicine, New York, NY 10029

Cellular morphogenesis, including polarized outgrowth, promotes tissue shape and function. Polarized vesicle trafficking has emerged as a fundamental mechanism by which protein and membrane can be targeted to discrete subcellular domains to promote localized protrusions. Frizzled (Fz)/planar cell polarity (PCP) signaling orchestrates cytoskeletal polarization and drives morphogenetic changes in such contexts as the vertebrate body axis and external *Drosophila melanogaster* tissues. Although regulation of Fz/PCP signaling via vesicle trafficking has been identified, the interplay between the vesicle trafficking machinery and downstream terminal PCP-directed processes is less established. In this paper, we show that *Drosophila* CK1-γ/*gilgamesh* (*gish*) regulates the PCP-associated process of trichome formation through effects on Rab11-mediated vesicle recycling. Although the core Fz/PCP proteins dictate prehair formation broadly, CK1-γ/*gish* restricts nucleation to a single site. Moreover, CK1-γ/*gish* works in parallel with the Fz/PCP effector *multiple wing hairs*, which restricts prehair formation along the perpendicular axis to Gish. Our findings suggest that polarized Rab11-mediated vesicle trafficking regulated by CK1-γ is required for PCP-directed processes.

Introduction

Cellular morphogenesis requires polarized vesicle trafficking and cytoskeletal rearrangements to promote asymmetric shape changes (Lecuit, 2003). Diverse cell types rely on polarized protrusive activity to perform specialized functions. In yeast, polarized vesicle trafficking directs membrane deposition to discrete regions during budding and mating (Madden and Snyder, 1998). Directed cell migration and neurite outgrowth require polarized trafficking for asymmetric cytoskeletal accumulation and expansion at the leading edge (Zhou and Cohan, 2004; Heasman and Ridley, 2008; Fletcher and Rappoport, 2009). Furthermore, ciliogenesis requires a polarized cytoskeleton and vesicle trafficking (Nachury et al., 2007; Yoshimura et al., 2007). Lastly, planar polarized cytoskeletal protrusions are required for the elongation of the body axis in convergent extension (Shih and Keller, 1992; Wallingford et al., 2002).

Frizzled (Fz)/planar cell polarity (PCP) signaling promotes the orientation of cells in vertebrate and invertebrate tissues (Adler, 2002; Klein and Mlodzik, 2005; Lawrence et al., 2007; Wang and Nathans, 2007; Wu and Mlodzik, 2009). In *Drosophila melanogaster*, Fz/PCP signaling controls the formation of single, distally oriented actin-based hairs (trichomes) on each wing cell (Wong and Adler, 1993). The core group of Fz/PCP proteins, including membrane-associated Fz, Flamingo (Fmi), and Strabismus (Stbm)/Van Gogh and cytoplasmic Dishevelled (Dsh), Diego, and Prickle, localize asymmetrically during the formation of polarized cells (Axelrod, 2001; Das et al., 2002; Strutt et al., 2002; Jenny et al., 2003; Rawls and Wolff, 2003; Das et al., 2004).

In the wing, a bias in Fz transport along microtubules has been proposed as a mechanism for asymmetric polarization and distal trichome placement along the proximodistal (PD) axis (Shimada et al., 2006; Harumoto et al., 2010). Several PCP signaling effectors restrict trichome number downstream of the core PCP proteins, including *Drosophila rho-associated kinase*

Correspondence to Marek Mlodzik: marek.mlodzik@mssm.edu

Abbreviations used in this paper: APF, after puparium formation; *Drok*, *Drosophila rho-associated kinase*; Dsh, Dishevelled; *en*, *engrailed*; Fmi, Flamingo; Fz, Frizzled; *gish*, *gilgamesh*; LOF, loss of function; MRLC, Myosin regulatory light chain; *mwh*, *multiple wing hairs*; *nub*, *nubbin*; *nuf*, *nuclear fallout*; PCP, planar cell polarity; PD, proximodistal; *pnr*, *pannier*; *sev*, *sevenless*; Stbm, Strabismus; TEM, transmission EM; UAS, upstream activation sequence; *zip*, *zipper*.

The Rockefeller University Press $30.00
J. Cell Biol. Vol. 196 No. 5 605–621
www.jcb.org/cgi/doi/10.1083/jcb.201107137

(*Drok*), *inturned*, *fuzzy*, and *multiple wing hairs* (*mwh*; Wong and Adler, 1993; Winter et al., 2001; Strutt and Warrington, 2008; Yan et al., 2008). However, the precise mechanism by which these effectors interact and coordinate single trichome formation with other cellular components is not well understood.

From a PCP modifier screen, we have identified and characterized the function of the *Drosophila* casein kinase 1 γ (CK1-γ) homologue *gilgamesh* (*gish*) in the regulation of trichome morphogenesis. Genetic analysis in *Drosophila* has revealed a role for CK1-γ/*gish* in glial cell migration (Hummel et al., 2002), olfactory learning (Tan et al., 2010), and sperm individualization, a process requiring membrane remodeling (Nerusheva et al., 2009). CK1-γ/*gish* is evolutionarily conserved, and the redundant yeast orthologues YCK1/YCK2 are essential for bud site selection, morphogenesis, and cytokinesis (Wang et al., 1992; Robinson et al., 1993). GFP-Yck2p localizes to sites of polarized bud growth (Lew and Reed, 1995; Robinson et al., 1999). CK1-γ requires C-terminal palmitoylation for membrane localization and function (Robinson et al., 1993; Vancura et al., 1994; Davidson et al., 2005). Therefore, evidence from yeast budding and *Drosophila* spermatogenesis suggests that CK1-γ/*gish* may regulate polarized membrane trafficking.

Here, we describe a function for CK1-γ/*gish* in the regulation of PCP-directed morphogenesis. We find that CK1-γ/*gish* and the PCP effector *mwh* cooperate in an independent manner to restrict trichome formation to a single cell site. CK1-γ/*gish* regulates Rab11-mediated polarized vesicle trafficking. In animal cells, Rab11 localizes to recycling endosomes and derived vesicles, where it regulates vesicle trafficking during such processes as cell migration (Mammoto et al., 1999; Jing et al., 2009) and cell polarization (Prekeris et al., 2000; Wang et al., 2000; Pelissier et al., 2003). We also find that CK1-γ/*gish* regulates the localization of Rab11 effectors *nuclear fallout* (*nuf*; Rab11-FIP3 homologue) and Sec15 (Riggs et al., 2003; Zhang et al., 2004; Langevin et al., 2005). *nuf* and Rab11 are mutually required for localization to the recycling endosome (Riggs et al., 2003), and *nuf* is required for microtubule-dependent trafficking of recycling endosomes (Riggs et al., 2007; Horgan et al., 2010). Sec15, a component of the exocyst complex, is associated with secretory vesicles and is required for polarized exocytosis (TerBush et al., 1996). In summary, our data support a model by which CK1-γ/*gish* regulates morphogenesis in development through the spatial control of polarized vesicle trafficking.

Results

gish, *Drosophila* CK1-γ, regulates cell and tissue morphogenesis

To identify genes involved in PCP establishment, we performed a genetic modifier screen using the DrosDel deficiency collection (unpublished data; Ryder et al., 2007). Overlapping deficiencies defined a region on chromosome 3R that enhanced the PCP defects (Materials and methods and unpublished data). Subsequent analysis using *upstream activation sequence* (*UAS*)-*RNAi* (*IR*) identified *gish* (unpublished data), the *Drosophila* CK1-γ homologue (Hummel et al., 2002).

Expression of $gish^{IR}$ under the control of *engrailed* (*en*)-*Gal4* (Fig. 1, B compare with A) or *FLP-FRT*–induced $gish^{e01759}$ (strong hypomorphic allele; Jia et al., 2005) mutant clones (Fig. 1 C) produced similar trichome defects. These results were confirmed with an independent RNAi sequence, $gish^{IR2}$ (also RNAi knockdown of the GFP fusion allele $gish^{spider\text{-}GFP}$ was observed by *en-Gal4 UAS-*$gish^{IR}$; Fig. S1, A [diagram] and B–C′′; Morin et al., 2001; Frescas et al., 2006).

To corroborate these results and determine the requirement of CK1-γ/Gish kinase activity, rescue experiments were performed. *en-Gal4* expression of the Myc-$Gish^{WT}$ transgene exhibited no phenotype (unpublished data), whereas its co-expression with $gish^{IR}$ partially rescued the trichome phenotype (Fig. S1, D, E and H, quantification). Two independent Myc-$Gish^{KD}$ lines (Fig. S1 A, diagram for D187N kinase-dead mutation) failed to rescue the $gish^{IR}$ phenotype (Fig. S1, F and H, quantification; and not depicted). Myc-$Gish^{\Delta C}$, a C-terminal truncation lacking the conserved palmitoylation site (Fig. S1 A), was ubiquitously localized and also failed to rescue the $gish^{IR}$ phenotype (Fig. S1, G and H, quantification). These data indicated that CK1-γ/Gish kinase activity and membrane association are required for trichome restriction.

Furthermore, to determine a general tissue requirement of CK1-γ/*gish* within the context of PCP, we analyzed whether trichome formation in the thorax results in the PCP morphogenetic process of ommatidial rotation in the eye. In the thorax, *pannier* (*pnr*)-*Gal4* expression of $gish^{IR}$ (Fig. 1, E compare with D) induced a phenotype with most cells projecting multiple trichomes (*fz* or *mwh* loss in the thorax and trichome orientation and morphogenesis defects; Krasnow and Adler, 1994; Olguín et al., 2011). Expression of $gish^{IR}$ in photoreceptors under the control of the *sevenless* (*sev*)-*Gal4* promoter or *FLP-FRT* $gish^{e01759}$ clones induced misrotated ommatial clusters (Fig. 1, G and H compare with F).

CK1-γ/*gish* restricts trichome formation by focusing actin nucleation

Just before prehair formation at 26–28 h after puparium formation (APF), much of the apical cell cortex consists of polymerized actin filaments (Eaton, 1997). At this stage, we observed no defects in actin polymerization in $gish^{IR}$ clones when compared with adjacent wild-type tissue (Fig. 2, A and A′). At 30–32 h APF, trichome formation appears at distal cell vertices as single focused actin-rich domains in wild-type tissue (Eaton, 1997). These domains often displayed multiple nucleation centers in $gish^{IR}$ clones (Fig. 2, B and B′, yellow arrowheads), indicating the primary defect in trichome morphogenesis occurred at this stage. These data suggested that the CK1-γ/*gish* loss-of-function (LOF) phenotype stemmed from a failure to restrict actin bundle nucleation to a single initiation site within the distal cell region. This was supported by later analysis (32–34 h APF), in which elongated trichomes displayed completely separate actin structures in CK1-γ/*gish* mutant cells (Fig. 2, C and C′, yellow arrowheads). This defect was observed in *FLP-FRT* $gish^{e01759}$ clones (Fig. S3, A and A′). This was also confirmed by transmission EM (TEM) on pupal wings expressing $gish^{IR}$ by *nubbin* (*nub*)-*Gal4*, which

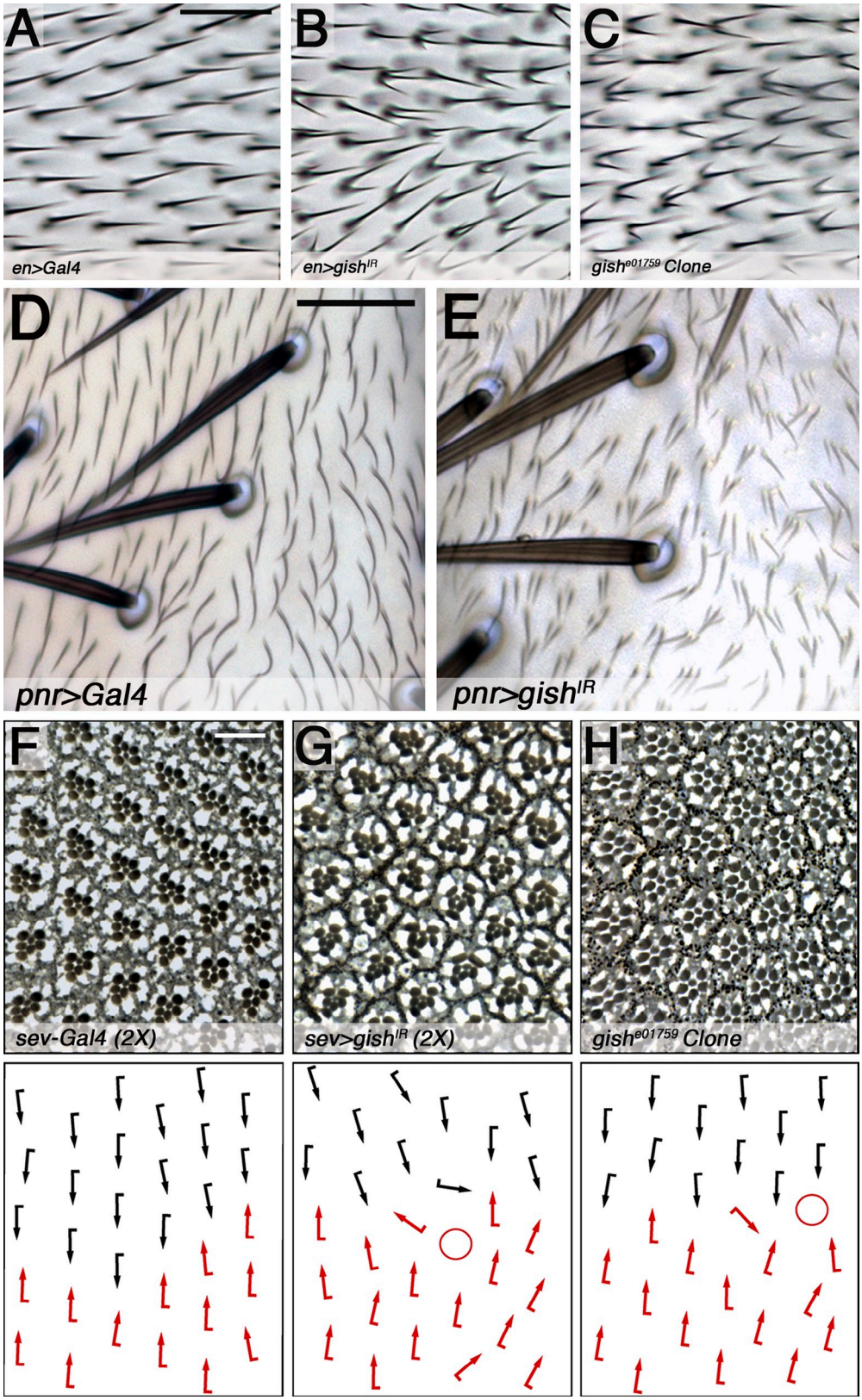

Figure 1. **CK1-γ/Gish regulates PCP-directed morphogenetic processes.** (A–C) Wild-type and *gish* LOF wings. All images show adult wings oriented with distal to the right. (A) Control, *engrailed* (*en*)-*Gal4*, displaying single distally oriented trichomes. (B and C) *en-Gal4 UAS-gish*^{IR} (B) and *FRT82-gish*^{e01759} clones (C) project multiple distally oriented trichomes. (D and E) Wild-type and *gish* LOF nota (dorsal thorax). Images show nota oriented with anterior to the top. (D) Control, *pannier* (*pnr*)-*Gal4* notum, exhibits single posterior-oriented trichomes. (E) Many cells in *pnr-Gal4 UAS-gish*^{IR} tissue project multiple trichomes. (F–H) Wild-type and *gish* mutant adult eye sections. (F) Homozygous *sevenless* (*sev*)-*Gal4* (*sev-Gal4* 2×) eyes display wild-type ommatidial orientation. (G and H) Homozygous *sev>gish*^{IR} (*sev>gish*^{IR} 2×; G) and *gish*^{e01759} clones (H) exhibit misrotated ommatidia. Anterior is to the left. Diagrams on the bottom depict rhabdomere orientation; circles represent irregular photoreceptor number. Bars: (A–C) 25 µm; (D and E) 50 µm; (F–H) 10 µm.

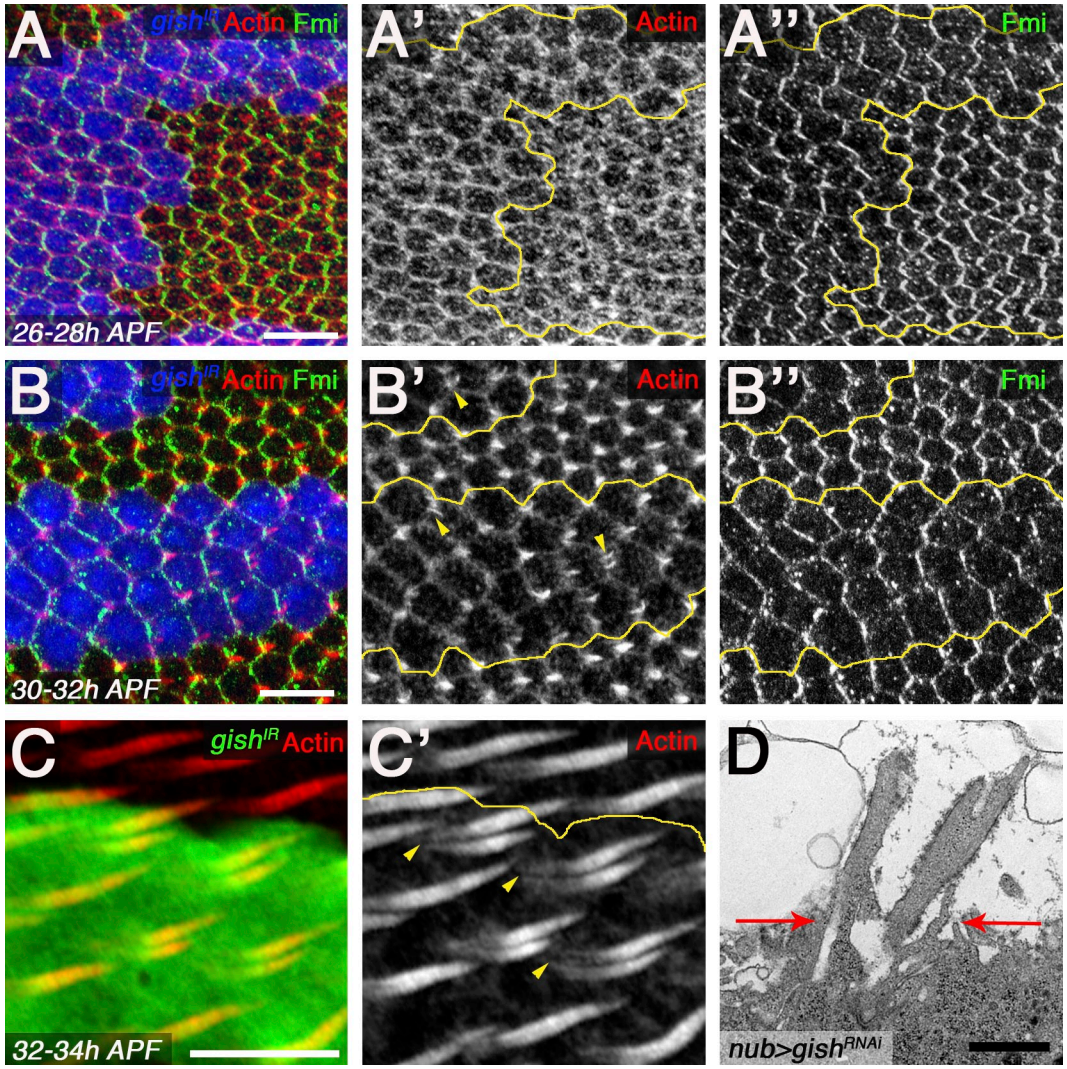

Figure 2. **Gish regulates single trichome nucleation.** (A–B′′) Pupal wing *actin-Gal4* FLP-out clones expressing *UAS-gish*^{IR} (blue; yellow lines mark clone border) stained with rhodamine-phalloidin (red) and Fmi. (A, A′, B, and B′) No defects in actin polymerization were observed from 26 to 28 h APF (A and A′), whereas multiple prehair nucleation sites can been observed at 30–32 h APF (B and B′, yellow arrowheads). (A′′ and B′′) Fmi localization is asymmetric in *gish*^{IR} tissue. (C–D) 32–34 h APF, independently nucleated actin prehairs are observed (C′, yellow arrowheads) and shown in a representative *nubbin* (*nub*)*-Gal4 UAS-gish*^{IR} TEM section (D, red arrows indicate apical cell surface). Bars: (A–C) 10 µm; (D) 1 µm.

revealed prehair separation to the apical cell surface (Fig. 2 D, red arrows).

Before prehair nucleation in wing cells, PCP proteins become asymmetrically localized through their interactions within the PD axis (Strutt and Strutt, 2009). Accordingly, mutations in core PCP genes result in symmetrical localization of the other PCP proteins (Strutt and Strutt, 2009). To determine whether CK1-γ/*gish* was required for PCP protein localization, we examined Fmi in *gish*^{IR} tissue and *gish*^{e01759} mutant clones. Asymmetric Fmi localization was not affected (Fig. 2, A′′ and B′′; and Fig. S3, A and compare C and C′ with B and B′). Collectively, our data support the hypothesis that CK1-γ/*gish* limits nucleation to a single location at the distal cell vertex through a mechanism downstream or in parallel to the core PCP components.

Interestingly, an increase in apical cell area was also observed in *gish*^{IR} tissue (Fig. S2, A–B′, compare green FLP-out clone with adjacent tissue). Measurement of the apical area revealed a 60% increase relative to the adjacent wild-type cells (Fig. S2, B–C), whereas analysis of the basolateral area did not show a significant increase (Fig. S2, B–C). TEM of wing cells expressing *gish*^{IR} revealed an increase in apical membrane projections (Fig. S2, D and E, compare boxed regions). From these observations, we suspected that the *gish*^{IR} phenotype was associated with decreased apical contractility or an increase in apical membrane trafficking. The defect was not associated with actomyosin dynamics, as the levels and localization of Myosin II heavy chain (Fig. S3, E–E′′) and activation of Myosin regulatory light chain (MRLC; Fig. S3 F) were not affected. Moreover, no modification of the *gish*^{IR} phenotype was observed when activated MRLC (Sqh^{EE}; Winter et al., 2001) was coexpressed (Fig. S2 C). These data suggested that expansion of the apical compartment was caused by increased membrane deposition. Support was generated

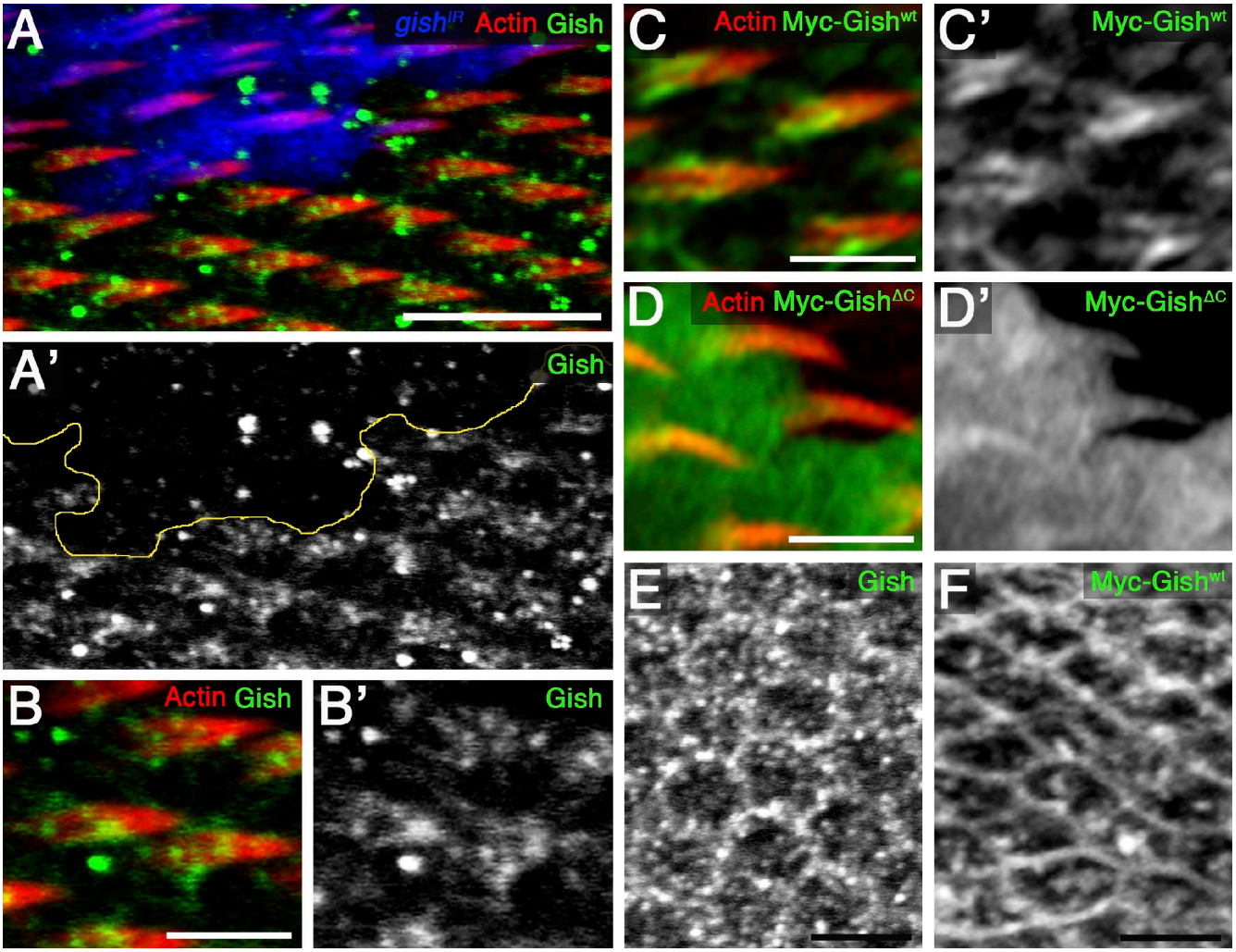

Figure 3. **CK1-γ/Gish is associated with the base of the developing trichome.** (A and A′) 32–34-h APF wing *actin-Gal4* FLP-out clones expressing *UAS-gish^{IR}* (blue; yellow line marks clone border). Endogenous Gish (green and monochrome in A and A′) is associated with the prehair base (prehair labeled with rhodamine-phalloidin, red). (B and B′) Magnified view of A and A′, outside *UAS-gish^{IR}* expression clone. (C–D′) 32–34-h APF pupal wings expressing *UAS-myc-gish^{WT}* or *UAS-myc-gish$^{\Delta C}$* in *actin-Gal4* FLP-out clones labeled with anti-Myc (green) and rhodamine-phalloidin (red). (C and C′) Gish is observed upon expression of Myc-Gish^{WT} (green or monochrome in C or C′). (D and D′) C-terminal truncation, Myc-Gish$^{\Delta C}$, is ubiquitously localized (green or monochrome in D or D′). (E and F) Basal projections of punctate and membrane localization of endogenous Gish (E) or Myc-Gish^{WT} (F) proteins. Bars: (A) 10 µm; (B–F) 5 µm.

from coexpression of activated Rab11^{CA} (Zhang et al., 2007), which enhanced *gish^{IR}*-induced membrane expansion (Fig. S2 C). This result was consistent with a role for Rab11 in apical membrane trafficking in polarized epithelial cells (Prekeris et al., 2000).

Because polyploid or enlarged cells have been shown in some cases to correlate with trichome defects (Adler et al., 2000), we analyzed the nuclear morphology of wing cells expressing *gish^{IR}* and also tested whether larger cells induced by other means displayed multiple trichomes. Cells expressing *gish^{IR}* had no observable change in intensity or area of nuclear staining compared with wild-type cells, indicating similar DNA content (Fig. S2, F, F′ [Hoechst], and G [quantification]). To generate larger cells, we expressed an RNAi against the tumor suppressor *PTEN* (Li et al., 1997). Similar to the enlarged cell phenotype associated with mutations such as *gigas* (Ito and Rubin, 1999), the increase in cell size of *PTEN^{IR}* did not affect trichome morphogenesis (Fig. S2, H and H′) or asymmetric Fmi localization (Fig. S2, H′′). Overall, these data suggest a direct role for CK1-γ/*gish* in regulating trichome formation.

CK1-γ/Gish localization during trichome morphogenesis

The CK1-γ/Gish protein was associated with the base of developing prehairs as observed in apical confocal projections of 32–34-h APF wings (Fig. 3, A and A′ and magnified in B and B′). Loss of staining in clones expressing *gish^{IR}* confirmed antibody specificity (Fig. 3, A and A′). A similar pattern was detected upon expression of Myc-Gish^{WT} (Fig. 3, C and C′). Myc-Gish^{KD} did not rescue the *gish^{IR}* phenotype (see previous section) but was enriched at the membrane (unpublished data). Lastly, Myc-Gish$^{\Delta C}$, which did not rescue *gish^{IR}* (see previous section), was ubiquitously localized in cells and prehairs (Fig. 3, D and D′). Analysis of subapical confocal projections (basal to prehair) revealed puncta and membrane

association for both endogenous and Myc-Gish^{WT} proteins (Fig. 3, E and F). In summary, CK1-γ/Gish is associated with the cell membrane and base of elongating prehairs.

CK1-γ/*gish* regulates trichome morphogenesis in parallel to the PCP pathway

Fz promotes trichome formation, and increased Fz levels result in multiple trichomes, likely through ectopic activation of the nucleation machinery (Krasnow and Adler, 1994). We reasoned that if the *gish*^{IR} phenotype resulted from Fz misregulation, removal of *fz* (null *fz*^{p21} allele) would reduce the *gish*^{IR} effect. We observed no change in the *gish* phenotype in the *fz*-null background (Fig. S3 D), suggesting that *gish* function is Fz independent. Furthermore, as *gish* LOF does not include trichome orientation defects, a characteristic of core PCP phenotypes, we hypothesized that *gish* may be linked to an effector cascade downstream of the core PCP group. We thus examined potential genetic relationships between *gish* and known effectors of the core PCP factors that control trichome number.

The *Drok*/*zipper* (*zip*) arm of PCP effector signaling failed to interact genetically with CK1-γ/*gish* (unpublished data). Furthermore, Zip localization or activation was not affected in *gish*^{IR} tissue (Fig. S3, E–F). We next analyzed the FH3 domain protein *mwh*, which is a PCP effector required to restrict actin filament formation and trichome number at the apical cell cortex (Wong and Adler, 1993; Strutt and Warrington, 2008; Yan et al., 2008). The null allele *mwh*^{1} dominantly enhanced the phenotype of *gish*^{e01759} homozygous mutant clones (Fig. 4, A and B). Coexpression of *mwh*^{IR} and *gish*^{IR} also resulted in a synergistic enhancement of trichome number as compared with expression of either RNAi alone (unpublished data). We expressed *gish*^{IR} in an *mwh*-null mutant background, reasoning that modification of the null phenotype would support a parallel relationship. Strikingly, expression of *gish*^{IR} strongly enhanced the *mwh*^{1}-null phenotype (Fig. 4, D–F, quantification). These data support a genetic model whereby CK1-γ/*gish* and *mwh* cooperate in a parallel manner to restrict trichome formation.

As CK1-γ/*gish* and *mwh* appeared to cooperate to restrict trichome formation in parallel, we wished to determine whether overexpression of one could suppress the defect of the other. Expression of either Mwh or Myc-Gish^{WT} alone had no phenotype (not depicted), whereas expression of Mwh strongly suppressed the *gish*^{IR} phenotype (Fig. 4, G, H, and M, quantification). Similarly, overexpression of Myc-Gish^{WT} suppressed the *mwh*^{IR} phenotype (Fig. 4, I, J, and M, quantification), whereas Myc-Gish^{KD} failed to do so (Fig. 4, K and M, quantification). Lastly, the ubiquitously localized Myc-Gish$^{\Delta C}$ (see previous section) also failed to suppress *mwh*^{IR} (Fig. 4, L and M, quantification). Collectively, these data suggest that *mwh* and CK1-γ/*gish* (via kinase activity and membrane localization) cooperate in a parallel to regulate trichome formation.

CK1-γ/*gish* regulates Rab11-mediated trafficking

The polarized localization of yeast CK1-γ to regions of membrane deposition/bud growth (Robinson et al., 1999), the morphogenesis phenotype of YCK1/YCK2 (Robinson et al., 1993), and the sperm individualization phenotype of *Drosophila* CK1-γ/*gish* (Nerusheva et al., 2009) support a role for CK1-γ in membrane dynamics (see Introduction). We hypothesized that CK1-γ/*gish* function in trichome morphogenesis was related to polarized membrane trafficking.

To test this hypothesis, we analyzed well-characterized markers, including the recycling endosome-associated Rab11 GTPase (Ullrich et al., 1996; Dollar et al., 2002; Pelissier et al., 2003). During early prehair formation (30–32 h APF), Rab11 was detected in puncta in the subapical region (Fig. 5 A′′ and Fig. S4 B, diagram) and was detected in strongly stained foci at the base of the initiating prehairs in the apical region (Fig. 5, A and A′, yellow arrowheads; and Fig. S4 B). Strikingly, the apical Rab11 foci were reduced from the prehair base of *gish*^{IR}-expressing cells, leaving mostly diffuse apical puncta (Fig. 5, A and A′). Abnormal Rab11 localization was also apparent in *gish*^{IR} clone tissue in 32–34-h APF wings; Rab11 was present uniformly in subapical cell regions in wild-type and *gish*^{IR} cells (Fig. 5, B′′ and D–D′′, z sections), but puncta detected along the length of the developing prehairs in wild-type cells (Fig. 5, B and B′, insets) were mostly absent in *gish*^{IR} cells (Fig. 5, B, B′, and E, quantification). Again, diffuse apical Rab11 staining remained in the *gish*^{IR} tissue (Fig. 4 B′). In support of these data, the Rab11 binding partner dRip11 (*Drosophila* class 1 Fip; Prekeris et al., 2000; Li et al., 2007) was enriched to the prehairs but appeared mislocalized in *gish*^{IR} tissue (Fig. S4, G and G′). The Rab11-interacting protein MyoV (Hales et al., 2002) did not localize to the prehairs (Fig. S4, F and F′), suggesting a context-specific association of these proteins. Furthermore, Rab11 localization is likely dependant on Gish kinase activity and membrane enrichment, as we detected a partial rescue of Rab11 localization only upon coexpression of the Gish^{WT} transgene in *gish*^{IR} tissue (Fig. S1, I–L′). These data suggested that CK1-γ/*gish* was required to enrich Rab11 endosomal structures to the developing prehairs.

As CK1-γ/*gish* and *mwh* interacted in trichome restriction, we tested whether *mwh* regulated Rab11 localization in a manner similar to CK1-γ/*gish*. *mwh*^{IR}-expressing cells exhibited normal Rab11 localization to elongating prehairs (Fig. 5, C, C′, and E, quantification). These data and the genetic analysis led us to conclude that the functions of CK1-γ/*gish* and *mwh* converge to regulate trichome morphogenesis but use distinct cellular mechanisms (see Discussion).

To confirm Rab11 localization and to visualize recycling endosome and vesicle dynamics near the prehairs, we performed in vivo imaging of YFP-Rab11^{WT} trafficking in the dorsal thorax (notum). At 36 h APF, we observed dynamic YFP-Rab11^{WT} foci enriched to the base and within the developing prehairs, as revealed by the membrane-associated CD8-RFP (Fig. 5 F and Video 1). In contrast, coexpression of *gish*^{IR} exhibited a diffuse YFP-Rab11 pattern (Fig. 5 G and Video 2), similar to endogenous Rab11. At 38 h APF, we observed trafficking of YFP-Rab11^{WT} within the elongating prehair (Fig. 5, H–J, yellow arrowheads; and Video 3). This activity was markedly reduced in the presence of a *gish*^{IR} trichome phenotype (Fig. 5, K–M, magenta arrowhead indicates remaining trafficking; and Video 4). These data support a requirement for *gish* in Rab11 dynamics associated with developing prehairs.

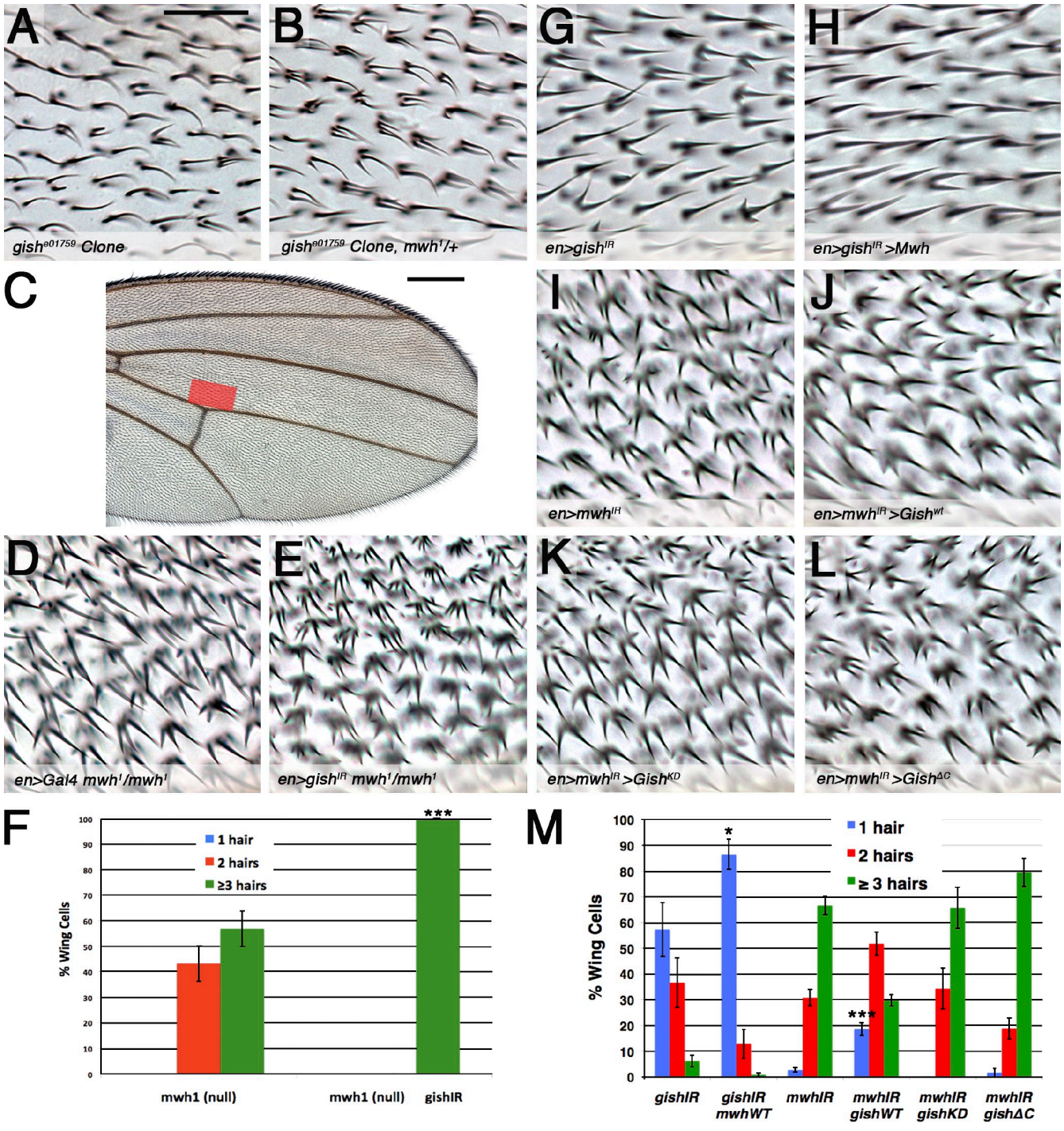

Figure 4. **CK1-γ/*gish* and PCP effector *mwh* function in a genetically independent manner to restrict trichome formation.** (A and B) The *FRT82-gish*^{e01759} mutant clone (A) is dominantly enhanced by the *multiple wing hairs* (*mwh*^{1})–null allele (B). (C) Wing hair number defects in D, E, and G–L were scored as a percentage of the total cells in the red highlighted region (D, E, and G–L are representative images of a smaller region within the red area). (D and E) *mwh*^{1}/*mwh*^{1}-null phenotype is enhanced by *en-Gal4 UAS-gish*^{IR} expression. (F) The quantification of results from D and E is represented. (G and H) The *en-Gal4 UAS-gish*^{IR} phenotype is strongly suppressed by coexpression of *UAS-mwh*. (I and J) *UAS-mwh*^{IR} was partially suppressed by *UAS-myc-gish*^{WT} coexpression. (K and L) Coexpression of *UAS-myc-gish*^{KD}, kinase-dead (KD; K), or the truncated/ubiquitously localized *UAS-myc-gish*$^{\Delta C}$ (L) failed to rescue the phenotype. (M) The quantification of results is represented. Error bars indicate SDs; unpaired *t* tests were performed on three independent animals (*, $P < 0.05$; ***, $P < 0.001$). WT, wild type. Bars: (A, B, and D–L) 25 µm; (C) 250 µm.

We extended the endosomal localization experiments to other markers of vesicle trafficking. In *gish*^{IR}-expressing cells, we found no defects in the level or localization of Rab5, which is required for early endocytic trafficking (Fig. S4, A–A′′; Bucci et al., 1992), the endosomal marker Hrs (Fig. S4, C–C′′; Lloyd et al., 2002), or the Golgi marker Lava Lamp (Fig. S4, D–D′′; Sisson et al., 2000). As studies in yeast have supported a role for CK1-γ in endocytosis (Panek et al., 1997; Marchal et al., 2000), we analyzed dextran uptake in third-instar wing disc FLP-out clones expressing *gish*^{IR} but observed no effects

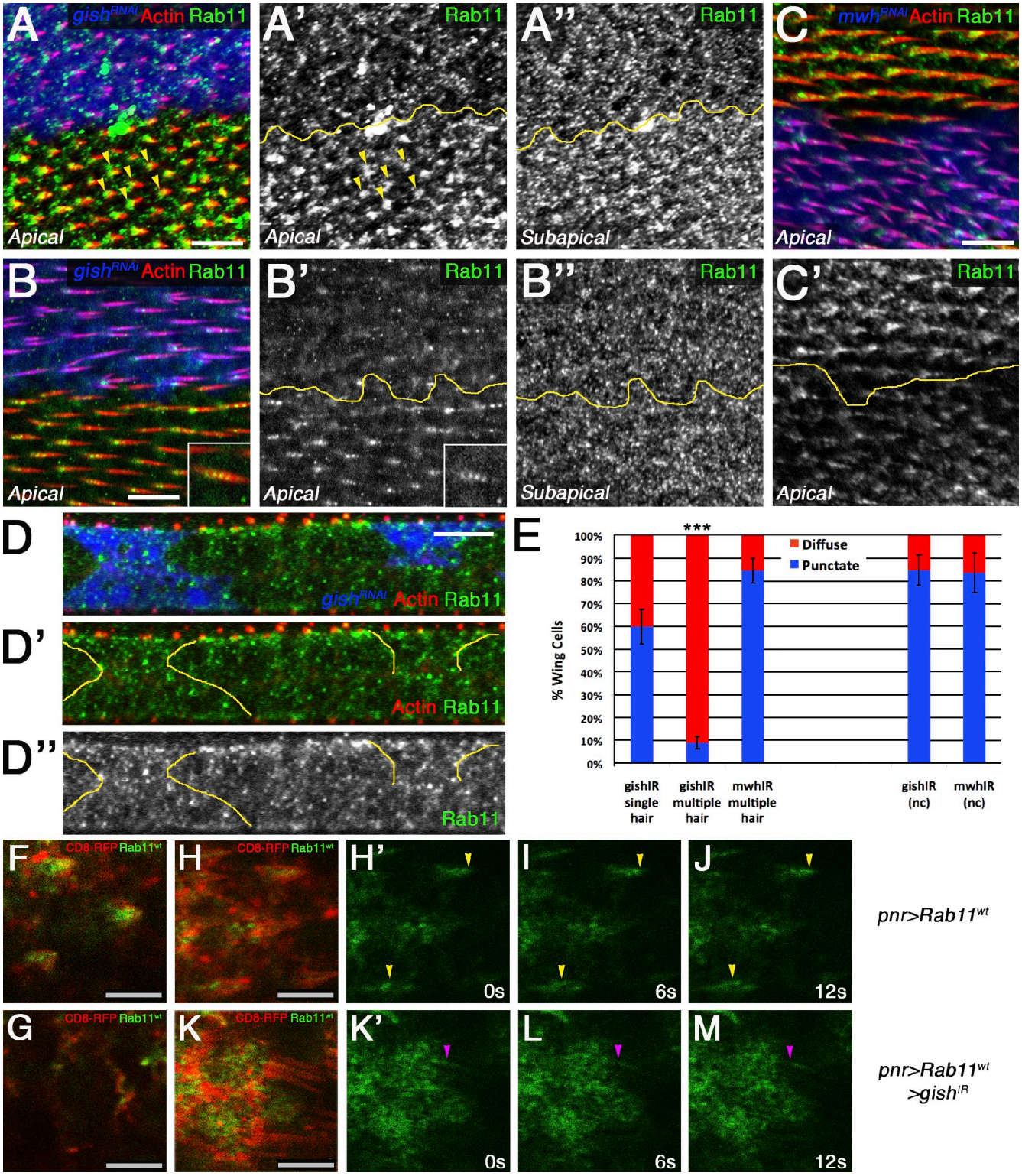

Figure 5. **CK1-γ/*gish* regulates dynamic apical Rab11 trafficking.** (A and A′) Endogenous Rab11 in apical confocal projections of 30–32-h APF pupal wings (Fig. S4 B, diagram). *actin-Gal4* FLP-out clones expressing *UAS-gish*^{IR} (blue) show an absence of Rab11 foci (green and monochrome in A and A′) at the trichome base (rhodamine-phalloidin, red; yellow arrowheads indicate Rab11 foci at the base of initiating prehairs). (A′′) Rab11 in subapical projections of the same *gish*^{IR} clones from A and A′. (B–B′′) In 32–34-h APF wings, Rab11 puncta (see insets) were absent within trichomes in *UAS-gish*^{IR} clones (blue; B and B′), whereas subapical regions appeared normal (B′′). (C and C′) *actin-Gal4* FLP-out clones of *UAS-mwh*^{IR} (blue) exhibit no effect on Rab11 localization (green and monochrome in C and C′). (D–D′′) Z sections of wings from B–B′′ (yellow lines indicate the *gishIR* clone border, which is blue in D). (E, left) Quantification of the percentage of cells with Rab11 puncta in multiple and single *gish*^{IR} mutant trichomes and multiple *mwh*^{IR} trichomes. (right) Rab11 detection in wild-type (nonclone [nc]) tissue is included to assess antibody/assay sensitivity. Error bars indicate SDs; unpaired *t* tests were performed on three independent animals (***, $P < 0.001$). (F–M) Time-lapse images of live notum epithelia highlighted with *pnr-Gal4* expressed *UAS-mCD8-RFP* to mark membranes and *UAS-YFP-Rab11*^{WT} labeling recycling endosomal structures. All images show nota oriented with anterior to the left.

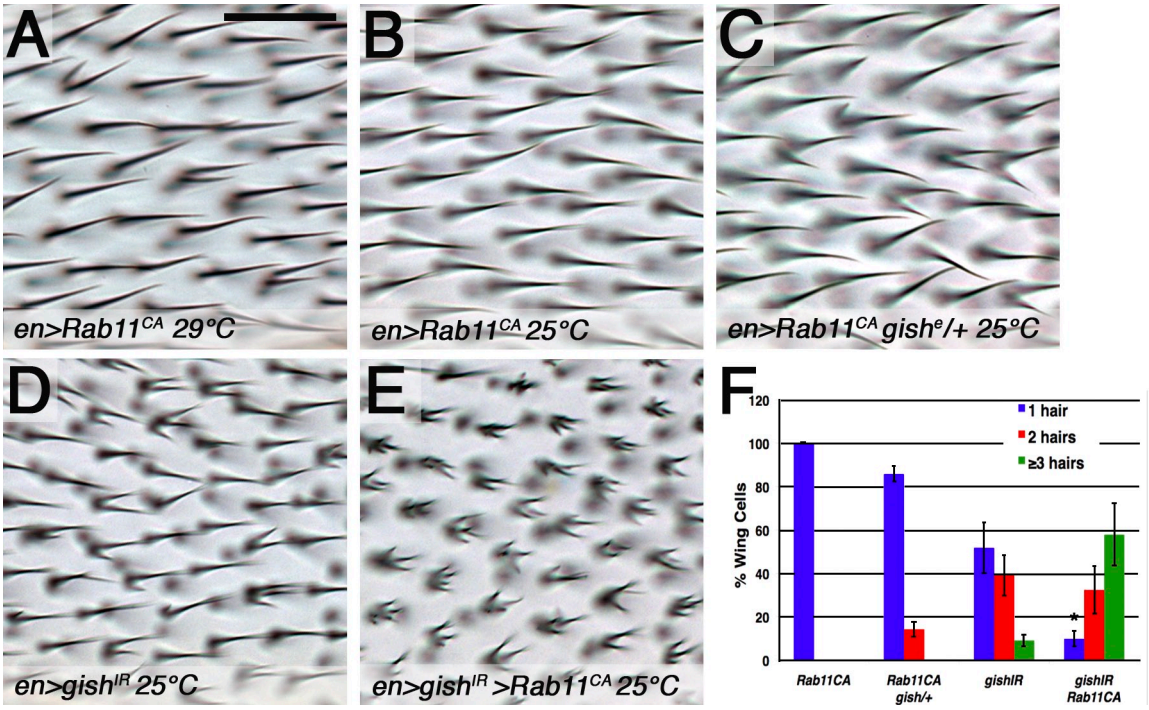

Figure 6. **CK1-γ/*gish* and Rab11 genetically interact during trichome formation.** (A) Strong expression of constitutively activated *en-Gal4 UAS-YFP-Rab11*^{CA} (29°C) resulted in multiple trichomes in adult wings. (B and C) *UAS-YFP-Rab11*^{CA} expression at 25°C via *en-Gal4* exhibited no phenotype (B), whereas a single allele of *gish*^{e01759} induced multiple trichomes (C). (D and E) The *en-Gal4 UAS-gish*^{IR} phenotype was synergistically enhanced by co-expression of *UAS-GFP-Rab11*^{CA} at 25°C. Distal is to the right in the images. (F) The quantification of results from B–E is represented. Error bars indicate SDs; unpaired *t* test was performed on three independent animals (*, P < 0.05). Bars, 25 µm.

(Fig. S4, E and E′). These results specifically implicate CK1-γ/*gish* in the regulation of Rab11/recycling endosomal (or vesicle) localization.

The failure to focus Rab11 in *gish*^{IR} cells supported the presence of a spatial bias in polarized trafficking within the distal cell vertex, which may be required for single trichome formation. To test this hypothesis, we reasoned that overexpression of a constitutively activated Rab11 (Rab11^{CA}; Zhang et al., 2007) might overwhelm the restriction and result in ectopic trichomes. Indeed, expression of YFP-Rab11^{CA} (29°C) in the posterior wing resulted in multiple trichomes (Fig. 6 A). We also tested for a genetic interaction between Rab11 and *gish*. Although lower expression of YFP-Rab11^{CA} (25°C) had no phenotype (Fig. 6 B), multiple trichomes were induced in a *gish*^{e01759} heterozygous background (Fig. 6, C and F, quantification). Consistently, coexpression of YFP-Rab11^{CA} and *gish*^{IR} exhibited a strong synergistic enhancement (Fig. 6, E and F, quantification) compared with either one alone (Fig. 6, B, D, and F, quantification). In contrast to Rab11, overexpression of Rab5^{CA} resulted only rarely in multiple trichomes, and Rab7^{CA} and Rab4^{CA} had no effect in our assay (unpublished data). In summary, our data indicate that CK1-γ/*gish* and Rab11 interact specifically during trichome formation.

To further dissect the *gish* and Rab11^{CA} interaction, we analyzed YFP-Rab11^{CA} localization in 32–34-h APF wing cells. Expression of *gish*^{IR} resulted in diffuse YFP-Rab11^{CA} localization (Fig. S5, B and B′), in contrast to focused Rab11^{CA} associated with control prehairs (Fig. S5, A and A′). These data indicated that the distribution of endogenous Rab11, YFP-Rab11^{WT}, and constitutively active YFP-Rab11^{CA} is altered in *gish*^{IR} cells. The enhancement of the Rab11^{CA} effect by *gish*^{IR} correlates with the diffuse localization of Rab11^{CA} away from the trichome. Furthermore, to determine the localization of Rab11 on an ultrastructural level, we analyzed the distribution of YFP-Rab11 in pupal wings by immuno-EM. In the pupal wing, YFP-Rab11 was observed in trichomes near the membrane (Fig. S5, E–E′′, black arrows), and abundant YFP-Rab11–positive areas were identified in the apical cell region (Fig. S5 F).

Rab11 and effectors are required for trichome formation

The model that *gish* enriches Rab11 vesicles to promote single trichomes suggests vesicle recycling is required to deliver trichome nucleation activity. Therefore, we analyzed the effect of decreasing Rab11 function. Expression of a dominant-negative Rab11,

(F) 36-h APF notum displays YFP-Rab11^{WT} localization to the base and within small prehairs (red). (G) The YFP-Rab11^{WT} pattern is lost upon *UAS-gish*^{IR} coexpression. (H) 38-h APF notum shows YFP-Rab11^{WT} (green) localization along the length of the prehair (red). (H′–J) Time-lapse images of YFP-Rab11^{WT} dynamics (yellow arrowheads mark initial position shown in H′ and serve as a reference in I and J). (K) 38-h APF notum coexpressing *UAS-gish*^{IR} displays diffuse YFP-Rab11^{WT} localization and rare trafficking in prehair (red). (K′–M) Time-lapse images tracking remaining YFP-Rab11^{WT} dynamics in prehair (magenta arrowheads mark trafficking shown in K′ and serve as a reference in L and M). Also see Videos 1, 2, 3, and 4. Yellow lines mark clone borders. Bars: (A–D) 10 µm; (F–H, and K) 5 µm.

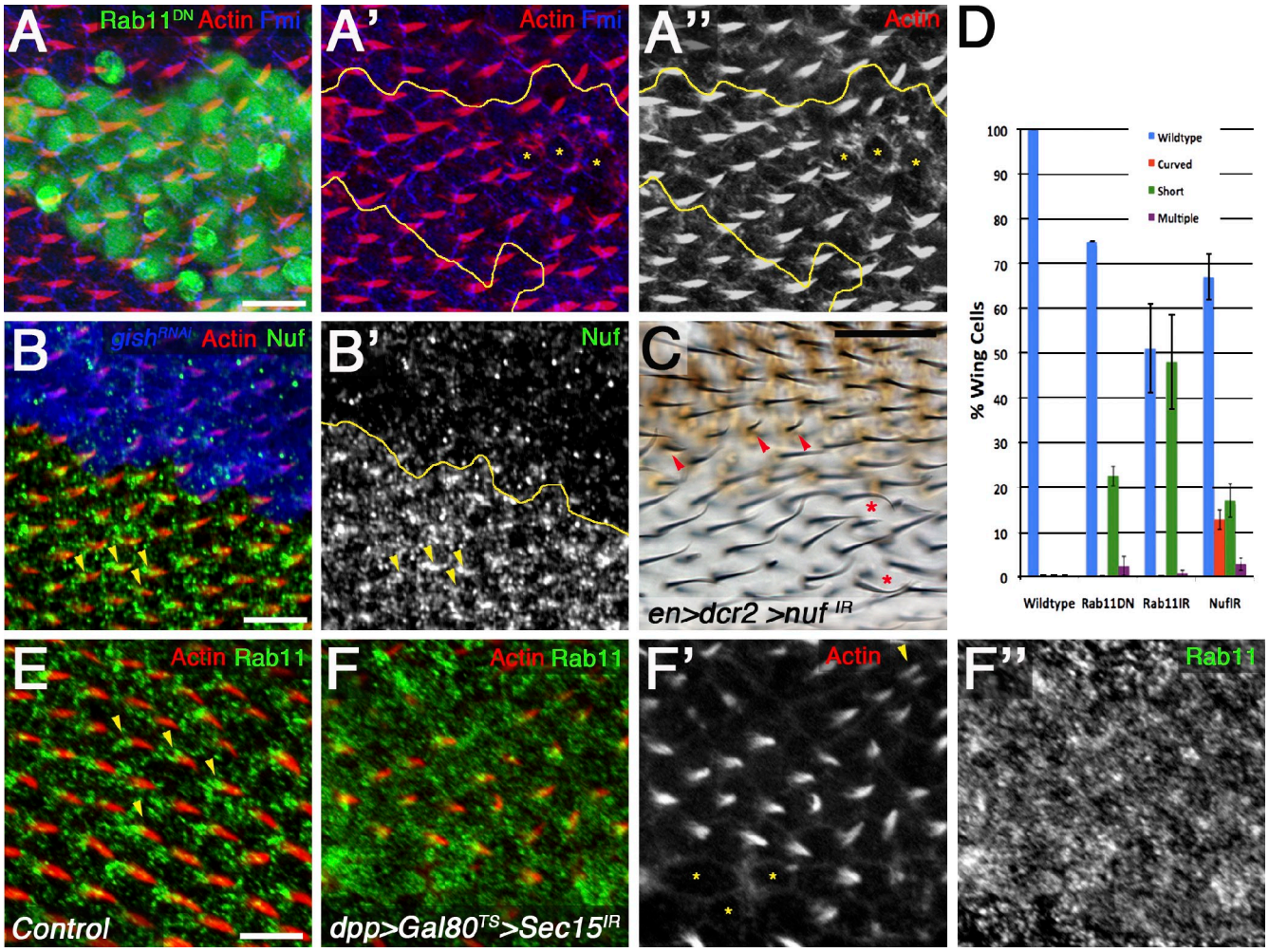

Figure 7. **Rab11 and effectors are required for trichome formation.** (A–A′′) 32–34-h APF pupal wings of *actin-Gal4* FLP-out clones expressing *UAS-YFP-Rab11*^{DN} (green; yellow lines mark clone border in A′ and A′′) display cells with short/missing prehairs (yellow asterisks in A′ and A′′; prehairs are red in A and A′ and monochrome in A′′). Cells are outlined with Fmi (blue in A and A′). (B and B′) 30–32-h APF wings of *actin-Gal4* FLP-out clones expressing *UAS-gish*^{IR} (blue; yellow line marks clone border) reveal dissociated Nuf foci (green and monochrome in B and B′) associated with the base of developing trichomes (red; yellow arrowheads indicate Nuf enriched at the base of the prehair). (C) *en-Gal4 UAS-dicer2 UAS-nuf*^{IR} adult wings display short (red arrowheads) or malformed (red asterisks) trichomes. (D) Quantification of the Rab11 and *nuf* LOF phenotypes was performed on three independent animals; error bars indicate SDs. (E) Control tissue adjacent to the *dpp* domain of *Sec15*^{IR} expression exhibits focused Rab11 localization (green) at the trichome base (red; yellow arrowheads indicate Rab11 enriched at the base of the prehair). (F–F′′) 32–34-h APF pupal wing expressing *dpp>Sec15*^{IR} after Gal80^{ts} temperature shift in third instar displays delayed or missing trichomes (red and monochrome in F and F′; yellow asterisks highlight examples of missing or shortened prehairs; the yellow arrowhead indicates an occasional multiple prehair) and accumulated/mislocalized endogenous Rab11 (green and monochrome in F and F′′). Bars: (A, B, E, and F) 10 µm; (C) 25 µm.

YFP-Rab11^{DN} (Zhang et al., 2007), or Rab11^{IR} (Vienna Drosophila RNAi Center; Satoh et al., 2005) in FLP-out clones resulted in cells with short/missing and malformed trichomes in pupal wings (Fig. 7, A–A′′ and D; Fig. S5, D and D′; and not depicted). We also confirmed Rab11 knockdown and antibody specificity in Rab11^{IR} FLP-out clones (Fig. S5, C and C′). Interfering with trafficking from the cell membrane to the early endosome via Rab5^{DN} resulted in trichome orientation and number phenotypes (unpublished data), consistent with the function of the Rab5 effector *rabenosyn-5* in PCP establishment (Mottola et al., 2010). Furthermore, interfering with late endocytic trafficking via Rab7^{DN} (Chavrier et al., 1990) or the fast endocytic recycling route through Rab4^{DN} (Van Der Sluijs et al., 1991) had no effect in our assay (unpublished data).

To further characterize the defects associated with recycling endosomal trafficking, we explored additional Rab11-associated proteins. The Rab11 effector *nuf* can bind Rab11 and link recycling endosome trafficking along microtubules via association with dynein (Riggs et al., 2007; Horgan et al., 2010). Nuf enrichment to the prehair base was dissociated in the apical domain of *gish*^{IR} tissue (Fig. 7, B and B′). We next explored the morphological effect of reducing Nuf by analyzing *nuf*^{IR} in adult wings. *nuf*^{IR} expression resulted in shortened or malformed trichomes (Fig. 7, C [arrowheads and asterisks] and D [quantification]). We also observed patches of missing trichomes (unpublished data). In addition, the exocyst component Sec15 is a downstream effector of Rab11 required for polarized membrane delivery (Langevin et al., 2005; Wu et al., 2005; Oztan et al., 2007). The Rab11–Sec15 complex is required to initiate the formation of the exocyst and promote tethering of recycling endosome–derived vesicles to the plasma membrane for subsequent membrane fusion (Wu et al., 2008).

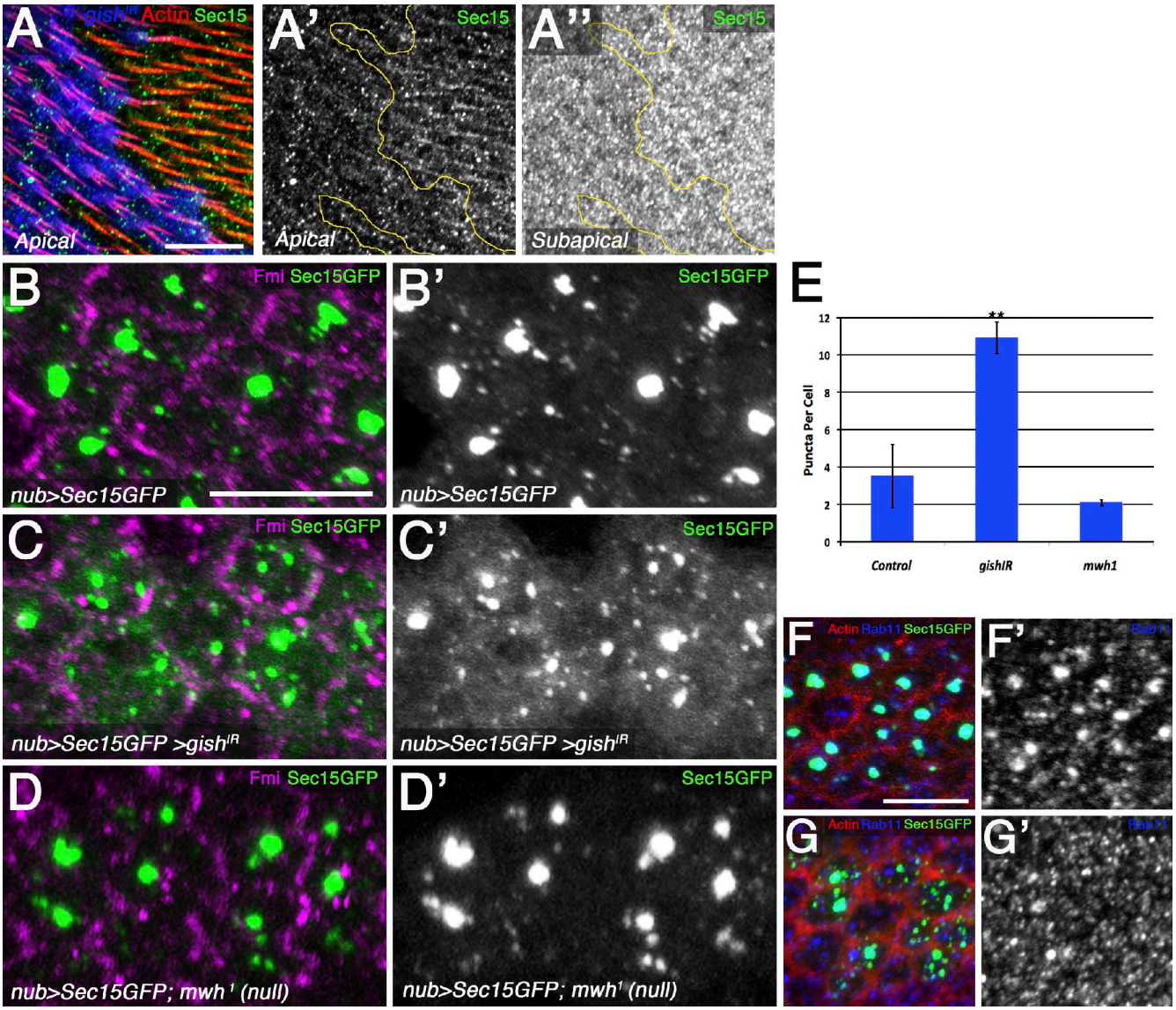

Figure 8. **CK1-γ/*gish* regulates Rab11 effector Sec15GFP.** (A–A′′) Endogenous Sec15 (green and monochrome) is reduced in apical *gish*^{IR} tissue (blue; yellow lines mark clone border). (B–C′) *nub-gal4 UAS-gish*^{IR} disrupts Sec15GFP aggregates in 30-h APF pupal wings (C and C′) compared with *nub-gal4* control tissue (B and B′; Fmi in magenta marks the membrane). (D and D′) The *mwh*^{1}-null allele has no effect on Sec15GFP aggregates. (E) Quantification of the mean number of Sec15GFP puncta per cell. Error bars indicate SDs; unpaired *t* testes were performed on three independent animals (**, $P < 0.01$). (F and F′) *nub-Gal4 UAS-Sec15GFP* expression in 30-h APF wings reveals large punctate colocalization of Sec15GFP and Rab11 (blue and monochrome in F and F′). (G and G′) *nub-Gal4* coexpression of *UAS-Sec15GFP and UAS-gish*^{IR} reveals dissociation of both Sec15GFP and Rab11 (blue and monochrome in G and G′). Bars, 10 µm.

We therefore analyzed the effect of reducing Sec15 function on trichome development. To circumvent early lethality, we initiated expression of *Sec15*^{IR} in third instar larval development. *Sec15*^{IR} induced defects in trichome development, similarly to Rab11 and Nuf, and, strikingly, caused an accumulation of Rab11 (see also Jafar-Nejad et al., 2005; Langevin et al., 2005) away from the base of the trichome across the cell (Fig. 7, compare E with F–F′′). Accumulated Rab11 and defective trichome formation in the context of Sec15 knockdown, in conjunction with the Rab11 and Nuf phenotypes displaying missing and malformed prehairs, reveal (a) a requirement for Rab11–Nuf–Sec15 trafficking in trichome formation and (b) a requirement for the Sec15–exocyst complex in localized trafficking of nucleation activity through the Rab11 recycling endosome to nucleation sites.

CK1-γ/*gish* regulates Rab11 effector Sec15

As *sec15*^{IR} exhibited effects on Rab11 localization and trichome formation, we analyzed the effect of *gish*^{IR} on endogenous Sec15. In 32–34-h APF wings, Sec15 was observed in a punctate distribution in the prehair, whereas apical Sec15 was mislocalized in *gish*^{IR} tissue (Fig. 8, A–A′′). Furthermore, large apical patches of aggregated vesicles (dependent on exocyst function) have been reported in yeast, *Drosophila* epithelia, and mammalian cells upon Sec15GFP expression (Salminen and Novick, 1989; Zhang et al., 2004; Guichard et al., 2010). Thus, as an assay for Sec15GFP localization/function, we analyzed the formation of these large puncta in pupal wing cells (Fig. 8, B, B′, and E, quantification). Strikingly, in *gish*^{IR} cells, we observed an overall

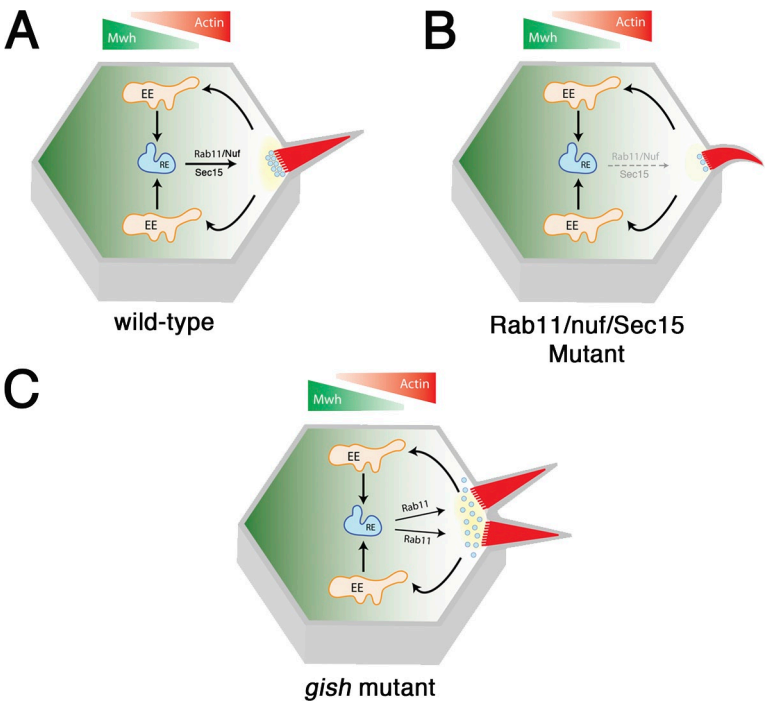

Figure 9. **Model of Gish/Rab11 vesicle trafficking during trichome formation.** (A) Model of *gish*-mediated vesicle trafficking during trichome formation. During prehair formation, two systems exist along orthogonal axes: (1) proximally enriched Mwh restricts actin nucleation along the proximal–distal axis, and (2) Gish directs the polarized trafficking and enrichment of Rab11 endosomes (and derived vesicles) to the prehair. Targeting of vesicle recycling restricts actin nucleation to a single site within the distal cell vertex. Polarized vesicle recycling to the proximity of the prehair base provides a mechanism whereby nucleation (yellow) is prevented from diffusing laterally, resulting in multiple trichomes. (B) Loss of Rab11–Nuf–Sec15 function results in reduced, absent, or abnormal trichome formation. (C) In *gish* mutant cells, focused Rab11–Nuf–Sec15 recycling is disrupted, resulting in diffuse membrane trafficking of nucleation activity and multiple trichome formation. EE, early endosome; RE, recycling endosomes.

dissociation of these large puncta (Fig. 8, C, C′, and E; and Fig. S4, H–I′), whereas *mwh*-null wings resembled the control (Fig. 8, D–E). Rab11 colocalized with Sec15GFP as previously reported (Zhang et al., 2004; Jafar-Nejad et al., 2005; Guichard et al., 2010), supporting that these structures were recycling vesicles trafficking to the plasma membrane (Fig. 8, F and F′). Sec15GFP and Rab11 were dissociated by $gish^{IR}$ (Fig. 8, G and G′). Collectively, our data suggest that CK1-γ/*gish* specifically regulates Rab11–Nuf–Sec15 vesicle localization and polarized trafficking between the recycling endosome and the plasma membrane.

Discussion

CK1-γ/*gish* regulates membrane trafficking to coordinate cell and tissue morphogenesis

Membrane trafficking is a key mechanism during morphogenesis and cell polarization (Lecuit, 2003; Mellman and Nelson, 2008). Studies in *Drosophila* have established a requirement for trafficking in core PCP protein localization, trichome orientation, and morphogenesis (Shimada et al., 2006; Strutt and Strutt, 2008; Fricke et al., 2009; Mottola et al., 2010; Pataki et al., 2010; Purvanov et al., 2010). Membrane trafficking has also been associated with PCP establishment in cell packing (Classen et al., 2005) and in vertebrate morphogenesis during cilia formation (Park et al., 1994; Gray et al., 2009). In the *Drosophila* wing, the core PCP proteins are required for the formation of a single trichome at the distal cell vertex, but these proteins are found along the entire distal (Fz/Dsh) and proximal (Stbm–Van Gogh/Prickle) cell sides (Adler, 2002). It is unclear how trichomes are restricted to one position within a broader PCP domain. It is likely that proteins, such as Fz, broadly define prehair formation and, within that domain, recruit the refinement proteins necessary to restrict the nucleation machinery to a central subdomain (Adler, 2002). The function of CK1-γ/*gish* in polarized vesicle trafficking provides a mechanism for refining a trichome to a single position.

Gish is localized to the cell periphery and the prehair base. This localization is consistent with a requirement for CK1-γ/*gish* in targeting nucleation activity to that region, as we have identified ectopic trichome nucleation as the primary defect. Moreover, our data implicate vesicle trafficking, as genetic alteration of Rab11 or effectors (*nuf* and Sec15) resulted in lost and/or malformed trichomes. Collectively, these data support a model that targeted membrane recycling through Rab11, Nuf, and Sec15 is required to build a trichome (Fig. 9, compare A and B), and spatial regulation of this trafficking by CK1-γ/*gish* is required to counteract lateral membrane localization of nucleation activity and ectopic trichome formation (Fig. 9, A and C). A similar model exists for polarized growth in yeast (e.g., bud growth), in which uptake and recycling is a mechanism to balance cdc42 lateral diffusion (Marco et al., 2007; Slaughter et al., 2009).

CK1-γ/*gish* coordinates membrane recycling through Rab11–Nuf–Sec15 vesicle trafficking

Our data provide evidence that Rab11–Nuf–Sec15 trafficking promotes trichome formation. Importantly, this study supports that CK1-γ/Gish regulates localized actin nucleation by directing Rab11–Nuf–Sec15-mediated vesicle trafficking between the recycling endosome and a distinct region of the membrane. Evidence for polarized recycling includes that (a) $Sec15^{IR}$ tissue displays trichome malformation in the presence of accumulated Rab11 vesicles away from the trichome base (reduced vesicle tethering and fusion can result in vesicle accumulation in the cell) and (b) dissociation of

Rab11–Nuf–Sec15 from the prehair in *gish*^{IR} cells is associated with multiple trichomes. These results suggest that polarized and focused membrane delivery of a nucleation factors may be disrupted. Interestingly, knockdown of the Arp2/3 nucleation machinery or regulators, such as Wasp, resulted in multiple trichomes (Fig. S5, G–I; Fricke et al., 2009) and can genetically enhance the *gish*^{IR} phenotype (Fig. S5, J–M, quantification). CK1-γ/Gish may promote delivery of Rab11–Nuf–Sec15 recycling vesicles carrying Arp2/3 activity to the prehair. Further experiments are needed to explore the relationship between localized Rab11 trafficking and the branched nucleation machinery.

As Gish is associated with the base of developing trichomes, it is possible that CK1-γ/*gish*, in analogy to the yeast homologue Yck2p, is localized to the proximal prehair membrane in an area of membrane deposition. Such localization suggests Gish could regulate localized trafficking by tethering Rab11 vesicles to the plasma membrane through the Sec15–exocyst complex. As in other contexts, Rab11 and Sec15 are functionally linked on vesicles en route from the recycling endosome to the plasma membrane. As *gish* reduction mislocalized endogenous Rab11–Nuf–Sec15 and dissociated the aggregated Sec15GFP and Rab11 colocalization pattern (but had no effect on alternative trafficking compartments, such as the Rab5 early endosome), this suggests CK1-γ/*gish* is required at a late vesicle recycling step. Although coimmunoprecipitation experiments with Myc-Gish failed to detect an association with Rab11, Nuf, or Sec15 (unpublished data), the potential phosphorylation targets may be binding partners or associate through weak/transient interactions with Gish.

Alternatively, CK1-γ/*gish* may regulate polarized vesicle trafficking through an effect on the cytoskeleton, associated motor proteins, or adaptors. As mentioned, the Rab11 effector Nuf can bind the motor protein dynein and link Rab11 endosomal structures to microtubules (Riggs et al., 2007; Horgan et al., 2010). A recent study showed that Nuf phosphorylation by IKK-ε regulates trafficking of Rab11 vesicles along developing bristles (Otani et al., 2011). Thus, one possibility is that CK1-γ/*gish* may act through Nuf to affect Rab11 trafficking. We have observed a correlation between Rab11 localization and microtubule networks within the prehair (unpublished data). Thus, Rab11 vesicles may require microtubules for localization, as previously reported in other contexts (Riggs et al., 2007). Consistent with this notion, microtubule depolymerization with nocodazole dissociated Sec15 vesicle aggregates in mammalian cells (Zhang et al., 2004). Intriguingly, disrupting microtubules resulted in multiple trichomes in *Drosophila* (Turner and Adler, 1998). Further analysis is necessary to address the role of *gish* on microtubule-based vesicle trafficking in the context of trichome formation.

CK1-γ/*gish* and *mwh* regulate distinct steps in trichome morphogenesis

PCP studies have identified effectors required to restrict trichomes, such as *fuzzy*, *inturned*, *frtz*, and *mwh* (Adler, 2002). Based on genetic epistasis and localization experiments, *mwh* is downstream as a modulator of the cytoskeleton (Wong and Adler, 1993; Strutt and Warrington, 2008; Yan et al., 2008). Mwh is enriched proximally, and a model has been proposed whereby prehair initiation is restricted to the distal cell region by the proximal repression of Mwh (and promoted by Fz in the distal domain). Taking these observations together with our data regarding the relationship of *mwh* and CK1-γ/*gish*, the restriction of prehair initiation requires two parallel mechanisms in orthogonal axes: (1) prehair initiation is restricted by the gradient of Mwh along the PD axis (e.g., wing) of the cell and (2) the tight restriction of Fz-directed trichome nucleation along a second axis of refinement by CK1-γ/*gish* (Fig. 9). This model is supported by both genetic and cell biological data: (a) analyses of CK1-γ/*gish* and *mwh* LOF reveal phenotypic differences—the initial prehair phenotype of CK1-γ/*gish* is restricted to the distal cell region and results in multiple, distally oriented trichomes, whereas the *mwh* phenotype is first observed as excess actin filaments over the entire apical cell cortex and results in multiple, randomly oriented trichomes (Strutt and Warrington, 2008), (b) *gish*^{IR} strongly enhances the *mwh*-null phenotype, indicative of two genetically independent pathways, and (c) CK1-γ/*gish* is required for Rab11 localization in the proximity of the developing prehair, whereas *mwh* has no effect on Rab11 (or Sec15GFP). Collectively, these data imply that these proteins perform two independent functions in the cell that converge to restrict trichome formation to a single site. In support of this model, our data indicate that excess of either of these proteins can partially suppress the defects associated with the loss of the other. Thus, we suspect a failure to focus trichome nucleation activity to the distal cell vertex by *gish* LOF can be corrected by increasing Mwh levels to repress actin nucleation/polymerization by an independent mechanism.

In summary, we define a novel mechanism by which trichome formation is restricted to a single domain in epithelial cells. These data support the model that CK1-γ kinases can regulate cellular morphogenesis through controlling the localization of Rab11 vesicle recycling. Our study has identified parallels between *Drosophila* and yeast CK1-γ in cellular morphogenesis, supporting a conserved mechanism of action. Collectively, our findings reveal that an independent mechanism of CK1-γ–regulated vesicle trafficking converges to refine Fz/PCP-directed morphogenesis.

Materials and methods

Fly stocks

Drosophila experiments were performed at 25°C unless otherwise indicated. Deficiency collection stocks used in the modifier screen were obtained from Exelixis, Szeged, and Bloomington Stock centers. Phenotypic analysis was performed on genes isolated in the modifier screen through transgenic UAS-RNAi flies obtained from the Vienna Drosophila RNAi Center (Dietzl et al., 2007). The following alleles were used in this study and obtained from the Bloomington Stock Center: *Drok*^{2}, *zip*^{1}, *gish*^{e01759}, *gish*$^{spider\text{-}GFP}$, *mwh*^{1}, and *scar*$^{\Delta 37}$ (described in Flybase). *wsp*^{3} was a gift from E.D. Schejter (Weizmann Institute of Science, Rehovot, Israel; Ben-Yaacov et al., 2001). *gish*^{e01759} is a transposon insertion allele and has been characterized as a strong hypomorphic mutation (Jia et al., 2005). *gish*^{e01759} was recombined onto an FRT82B chromosome, and mitotic clones of FRT82B-*gish*^{e01759} were generated via the FLP/FRT system (Xu and Rubin, 1993). Clones were unmarked or marked with the *forked* mutation in adults or marked by the absence of β-galactosidase in pupal tissue. *gish*$^{spider\text{-}GFP}$ is a

protein trap insertion within the *gish* locus, generating a Gish-GFP fusion protein (Morin et al., 2001; Frescas et al., 2006). Overexpression of cDNA transgenes or RNAi (*IR*) was performed using the Gal4/UAS system (Brand and Perrimon, 1993). The Gal4 expression drivers used were as follows: *sev-Gal4*, *en-Gal4*, *nub-Gal4*, and *dpp-Gal4*. FLP-out expression clones of the indicated genotypes were performed using *hs-FLP; actin>y>Gal4, UAS-GFP* (Struhl and Basler, 1993). *UAS-gish^{IR}* (v26003), *UAS-mwh^{IR}* (v41514), *UAS-Rab11^{IR}* (v22198), *UAS-Sec15^{IR}* (v105126), and *UAS-PTEN^{IR}* (v35731) were obtained from the Vienna Drosophila RNAi Center collection. Where indicated, *UAS-dicer2* was included with *UAS-IR* expression to increase RNAi efficiency (Bloomington Stock Center). The following transgenes were also used: *UAS-sqh^{E20E21}* (Winter et al., 2001), *UAS-mwh* (Yan et al., 2008), *UAS-Sec15GFP* (Jafar-Nejad et al., 2005), *UAS-Rab11^{IR}* (Satoh et al., 2005), *UAS-YFP-RabGTPases* (including wild type, dominant negative, and constitutively active; Zhang et al., 2007), *arm-fz-GFP* (Strutt, 2001), *actin-stbm-YFP* (Strutt et al., 2002), and *UAS-kette^{Myr}* (Bogdan and Klämbt, 2003). Temperature shifting experiments were performed via an 18–29°C shift during the third-instar larval stage using the *tub-Gal80^{ts}* transgene (Bloomington Stock Center).

Molecular cloning

The following transgenes were generated from the Berkeley Drosophila Geneome Project *gish* cDNA clone LD04357: *UAS-gish^{IR2}* was created by PCR amplifying a cDNA sequence (independent of the Vienna Drosophila RNAi Center probe sequence; Fig. S1 A) into a modified pWizDir vector (Jenny and Mlodzik, 2008). The PCR primers used to generate *gish^{IR2}* were (including restriction sites) forward, 5′-ATCCCTAGGCTCCACCGGATCGAATATGTT-3′, and reverse, 5′-GCTGGATCCCACCGATTTTTTGATATCTCT-3′. *UAS-myc-gish^{WT}* and *UAS-myc-gish$^{\Delta C}$* were PCR isolated and correspond to transcripts *gish-RB* and *gish-RF*, respectively (described in Flybase). The PCR primers used to generate these transcripts were (including restriction sites and linkers) forward primer (common for *gish-RB* and *gish-RF*), 5′-ATCGAATTCGGCGGCATGCAGCGACGAGAACGGCAA-3′, reverse (*gish-RB* only), 5′-GCTCTCGAGTCATTTTTGGCGCGTCGATTT-3′, and reverse (*gish-RF* only), 5′-GCTCTCGAGCTATGTCTCCATTGTCTTCCC-3′. These PCR products were cloned into pCS2-Myc, and *myc-gish* was subcloned into the pUAST vector to generate transgenic flies. *myc-gish^{KD}* (D187N substitution) was generated by site-directed mutagenesis (Agilent Technologies) of pCS2-m*yc-gish^{WT}* followed by subcloning of *myc-gish^{KD}* into pUAST. The PCR primers used to generate the D187N substitution were forward, 5′-GGCACTTAATATATAGG**AAT**GTGAAACCAGAGAAC-3′, and complementary reverse, 5′-GTTCTCTGGTTTCAC**ATT**CCTATATATTAAGTGCC-3′. Substituted nucleotides are in bold. The *gish* kinase-dead D187N mutation is based on the comparable *Xenopus laevis* CK1-γ mutant on a conserved residue in the ATPase domain (Davidson et al., 2005).

Immunohistochemistry and histology

For analysis of wing trichomes, adult wings were removed, incubated in wash buffer (PBS and 0.1% Triton X-100), and mounted on a slide in 80% glycerol in PBS. To analyze trichomes in adult nota (dorsal thorax), flies were partially dissected, incubated at 95°C in 10% KOH for 10 min to clear fat tissue, washed (PBS and 0.1% Triton X-100), and then placed in 80% glycerol in PBS. Nota were then fully dissected and mounted on a slide in 80% glycerol in PBS. Adult eye section analyses were performed as previously described (Gaengel and Mlodzik, 2008). In brief, fly heads were fixed in 2% glutaraldehyde in PBS and treated with 2% osmium tetroxide. Samples were dehydrated in a graded ethanol series (50, 70, 90, and 100%) and propylene oxide and embedded in Durcupan resin. Tangential sections were made and mounted on a slide using DPX mounting medium. Adult wings, nota, and eye sections were imaged at room temperature on a microscope (Axioplan; Carl Zeiss). Images were acquired with a camera (Zeiss AxioCam Color type 412–312; Carl Zeiss) and AxioCam software. For analysis of pupal wings, white pupae were collected (0 h APF) and aged at 25°C. Dissections were performed as follows: in brief, pupae were immobilized on double-sided tape, removed from the pupal case, and placed into PBS, in which pupae were partially dissected to remove fat tissue and then fixed in 4% formaldehyde in PBS and washed three times (PBS and 0.1% Triton X-100). Wing membranes were removed, and tissue was incubated in wash buffer containing 10% normal goat serum overnight for primary antibody (4°C), washed three times with PBS, and then incubated with secondary for 1 h (25°C). Wings were washed three times with PBS and mounted in glycerol/PBS supplemented with 1% *N*-propyl gallate. Pupal wing images were acquired at room temperature using a confocal microscope (63×, 1.4 NA; LSM 510 Meta; Carl Zeiss) using LSM software (Carl Zeiss). Images were processed with ImageJ (National Institutes of Health) and Photoshop (CS4; Adobe).

Antibodies

Rabbit anti–β-galactosidase (1:1,000; European Molecular Biology Laboratory), rat anti-Rab11 (Dollar et al., 2002), rabbit anti-Rab5 (1:1,000; ab31261; Abcam), guinea pig anti-Hrs (Lloyd et al., 2002), guinea pig anti-Sec15 (1:500; Mehta et al., 2005), rabbit anti–Lava lamp (Sisson et al., 2000), mouse anti-Fmi (1:10; Developmental Studies Hybridoma Bank), rabbit anti-MyoV (1:1,000; Li et al., 2007), rabbit anti-dRip11 (1:1,000; Li et al., 2007), rabbit anti-Sec5 (Murthy et al., 2003), rabbit anti-Nuf (1:1,000; Riggs et al., 2003), mouse anti-Myc (1:250; 9E10; Santa Cruz Biotechnology, Inc.), mouse anti-En (1:2; Developmental Studies Hybridoma Bank), rabbit anti-Zip (Liu et al., 2008), and rabbit anti-GFP (1:1,000; Invitrogen). Rhodamine-phalloidin was obtained from Invitrogen. All fluorophore-conjugated secondary antibodies, including Cy5, TRITC, and FITC, were used at 1:200 and were obtained from Jackson ImmunoResearch Laboratories, Inc. Donkey anti–rabbit 10-nm gold was used at 1:200 (ab27235; Abcam).

Image analysis

Cell area measurements were performed using ImageJ. The apical cell periphery was identified by Fmi staining (overlapping apical adherens junctions), and basolateral area measurements were identified by rhodamine-phalloidin staining of cortical actin basal to nuclear level (Hoechst 33342; Thermo Fisher Scientific). Individual cell membranes were traced using the polygon drawing tool, and measurements were determined. Measurements were performed on ≥30 cells for control and adjacent mutant tissue (32–34 h APF). The percent increase of the area of mutant tissue was calculated relative to adjacent control tissue in the same wing. Means and SDs were calculated from at least three wings from individual animals. Sec15GFP puncta number per cell was determined using the particle analysis function of ImageJ. Three independent wings were analyzed, and the number of Sec15GFP-positive cells in each field was used to determine the mean number of puncta per cell.

Live imaging of pupal notum

White pupae (0 h APF) of the indicated genotypes were collected into separate vials, aged to 36 or 38 h APF at 25°C, and mounted for imaging as previously described (Bellaïche et al., 2001). In brief, aged pupae were fixed on slides with double-sided tape in between stacks of four coverslips. Pupal cases were partially removed to expose head and notum. A drop of halocarbon oil (Sigma-Aldrich) was placed onto the bottom of a cover slide and gently applied to the notum, supported by the adjacent stacks of coverslips. Images were acquired at room temperature using a confocal microscope (63× oil immersion, 1.4 NA; SP5 DMI; Leica) with LAS AF (Leica) software. A single confocal plane (1 µm) was taken at 6-s intervals for a total of 2 min.

Dextran uptake assay

The dextran uptake assay was performed as previously described (Entchev et al., 2000) with some modifications: third-instar larvae were partially dissected in S2 medium supplemented with 10% FBS to expose wing discs. The medium was replaced with one containing 5 mg/ml Texas red dextran (lysine fixable; 3,000 molecular weight; Invitrogen) and pulsed for 10 min at 25°C. The samples were washed three times with ice-cold S2 medium (with 10% FBS) and then incubated at 25°C for 20 min (chase) to visualize uptake and the early endosomal compartment. The samples were fixed for 20 min in 4% formaldehyde in PBS and washed three times in PBS with 0.1% Triton X-100. Mounting was in 30% glycerol (Mowiol and 2.5% Dabco). Images were acquired at room temperature using a confocal microscope (63×, 1.4 NA; LSM 510 Meta) using LSM software. Images were processed with ImageJ and Photoshop CS4.

EM

White pupae (0 h APF) of the indicated genotypes were isolated and staged to 32 h APF, and pupal wings were dissected as described in Immunohistochemistry and histology. Wings were fixed in 3% glutaraldehyde and then in 1% osmium tetroxide. Samples were dehydrated in a graded ethanol series (50, 70, 90, and 100%) and propylene oxide and embedded in Epon resin. Ultrathin sections were made along oblique angles to the apical epithelial surface of pupal wing epithelia. Immuno-EM sample preparation was as previously described (Shimada et al., 2006). In brief, white pupae (0 h APF) of the indicated genotype was isolated, staged to 32 h APF, dissected in PBS, and fixed for 1 h in periodate-lysine-paraformaldehyde fix. Pupae were washed three times in PBS. Blocking was performed by incubation for 1 h in glycine-PBS supplemented with 4% normal donkey serum, 0.1% saponin, and 0.05% Triton X-100. The primary antibody was diluted in blocking solution and incubated overnight

at 4°C. Pupae were washed five times in glycine-PBS and then incubated for 3 h with secondary antibody and washed five times. All subsequent steps were as described in the previous paragraph for standard TEM. The electron microscope used in all cases was an H-7650 (Hitachi) with MaxIm DL software (Diffraction Ltd.).

Immunoblotting

Third-instar wing imaginal discs (50 discs/genotype) were dissected and placed directly into SDS sample buffer to dissolve the tissue. These samples were boiled at 95°C for 10 min and then centrifuged at 14,000 rpm for 10 min. The supernatant was run on a 10% SDS-PAGE gel and transferred to polyvinylidene fluoride membrane (Millipore). The membranes were probed with rabbit antiphospho-MRLC (Ser19; Cell Signaling Technology). ECL Plus was used for detection (GE Healthcare).

Cell culture and siRNA

293T cells were cultured in DME supplemented with 10% FBS and maintained in 5% CO_2 at 37°C. Cells were transfected with siRNA against human CSNK1G1, CSNK1G2, and CSNK1G3 or negative control siRNA (Silencer Select siRNA and negative control #1; Invitrogen). Transfection was performed using siPORT *NeoFX* (Invitrogen). After 48 h, cells were transfected with pEGFP-Sec15GFP (0.4 µg per well; 8-well Laboratory-Tek glass chamber slide; a gift from C.A. Mitchell, Monash University, Clayton Victoria, Australia; Zhang et al., 2004) with the transfection reagent (FuGENE HD; Promega). After 24 h, cells were fixed with 4% paraformaldehyde, washed in PBS (0.1% Triton X-100), and mounted with Vectashield (including DAPI; Vector Laboratories). Images were acquired using a confocal microscope (63×, 1.4 NA; LSM 510 Meta) using LSM software. Images were processed with ImageJ and Photoshop CS4.

Online supplemental material

Fig. S1 shows in vivo RNAi strategy used for *gish* knockdown and the requirement for CK1-γ/Gish kinase activity and membrane association in trichome formation and Rab11 localization. Fig. S2 displays data characterizing the apical membrane expansion phenotype of $gish^{IR}$. Fig. S3 displays data supporting a PCP-independent role for CK1-γ/*gish* in trichome morphogenesis. Fig. S4 shows control stainings of additional trafficking compartments and Rab11-associated proteins. Fig. S5 shows the effect of *gish* on YFP-$Rab11^{CA}$ localization, YFP-$Rab11^{WT}$ localization in the context of trichome formation by immuno-EM, $Rab11^{IR}$ knockdown of endogenous Rab11, and genetic data implicating Arp2/3 nucleators in *gish* regulation of trichome morphogenesis. Video 1 shows YFP-$Rab11^{WT}$ trafficking within initiating prehair in a 36-h APF notum. Video 2 shows diffuse localization of YFP-$Rab11^{WT}$ with $gish^{IR}$ coexpression in a 36-h APF notum. Video 3 shows YFP-$Rab11^{WT}$ trafficking within elongating prehair in a 38-h APF notum. Video 4 shows diffuse YFP-$Rab11^{WT}$ trafficking with $gish^{IR}$ coexpression during prehair elongating in a 38-h APF notum. Online supplemental material is available at http://www.jcb.org/cgi/content/full/jcb.201107137/DC1.

We are grateful to Paul Adler, Hugo Bellen, William Sullivan, Ken Prehoda, Jennifer Zallen, Thomas Schwarz, Christina Mitchell, Robert Cohen, Ronald Davis, Donald Ready, Nicholas Baker, and the Bloomington, Exelixis, Szeged, and Vienna Drosophila RNAi Center stock centers for fly stocks and reagents. We thank Jeffery Bush, Robert Krauss, and Alvaro Glavic for advice and critical reading of the manuscript and members of the Mlodzik laboratory for critical comments and support. We also thank Suzanna Franks for diagrams and Aurore Dussert, Andrea Blitzer, and Sarah McGowan for technical support.

This work was supported by National Institutes of Health grant GM62917 to M. Mlodzik. W.J. Gault was also supported by award number T32CA078207 from the National Cancer Institute.

Submitted: 26 July 2011
Accepted: 2 February 2012

References

Adler, P.N. 2002. Planar signaling and morphogenesis in *Drosophila*. *Dev. Cell*. 2:525–535. http://dx.doi.org/10.1016/S1534-5807(02)00176-4

Adler, P.N., J. Liu, and J. Charlton. 2000. Cell size and the morphogenesis of wing hairs in *Drosophila*. *Genesis*. 28:82–91. http://dx.doi.org/10.1002/1526-968X(200010)28:2<82::AID-GENE60>3.0.CO;2-Z

Axelrod, J.D. 2001. Unipolar membrane association of Dishevelled mediates Frizzled planar cell polarity signaling. *Genes Dev.* 15:1182–1187.

Bellaïche, Y., M. Gho, J.A. Kaltschmidt, A.H. Brand, and F. Schweisguth. 2001. Frizzled regulates localization of cell-fate determinants and mitotic spindle rotation during asymmetric cell division. *Nat. Cell Biol.* 3:50–57. http://dx.doi.org/10.1038/35050558

Ben-Yaacov, S., R. Le Borgne, I. Abramson, F. Schweisguth, and E.D. Schejter. 2001. *Wasp*, the *Drosophila* Wiskott-Aldrich syndrome gene homologue, is required for cell fate decisions mediated by *Notch* signaling. *J. Cell Biol.* 152:1–13. http://dx.doi.org/10.1083/jcb.152.1.1-b

Bogdan, S., and C. Klämbt. 2003. Kette regulates actin dynamics and genetically interacts with Wave and Wasp. *Development*. 130:4427–4437. http://dx.doi.org/10.1242/dev.00663

Brand, A.H., and N. Perrimon. 1993. Targeted gene expression as a means of altering cell fates and generating dominant phenotypes. *Development*. 118:401–415.

Bucci, C., R.G. Parton, I.H. Mather, H. Stunnenberg, K. Simons, B. Hoflack, and M. Zerial. 1992. The small GTPase rab5 functions as a regulatory factor in the early endocytic pathway. *Cell*. 70:715–728. http://dx.doi.org/10.1016/0092-8674(92)90306-W

Chavrier, P., R.G. Parton, H.P. Hauri, K. Simons, and M. Zerial. 1990. Localization of low molecular weight GTP binding proteins to exocytic and endocytic compartments. *Cell*. 62:317–329. http://dx.doi.org/10.1016/0092-8674(90)90369-P

Classen, A.K., K.I. Anderson, E. Marois, and S. Eaton. 2005. Hexagonal packing of *Drosophila* wing epithelial cells by the planar cell polarity pathway. *Dev. Cell*. 9:805–817. http://dx.doi.org/10.1016/j.devcel.2005.10.016

Das, G., J. Reynolds-Kenneally, and M. Mlodzik. 2002. The atypical cadherin Flamingo links Frizzled and Notch signaling in planar polarity establishment in the *Drosophila* eye. *Dev. Cell*. 2:655–666. http://dx.doi.org/10.1016/S1534-5807(02)00147-8

Das, G., A. Jenny, T.J. Klein, S. Eaton, and M. Mlodzik. 2004. Diego interacts with Prickle and Strabismus/Van Gogh to localize planar cell polarity complexes. *Development*. 131:4467–4476. http://dx.doi.org/10.1242/dev.01317

Davidson, G., W. Wu, J. Shen, J. Bilic, U. Fenger, P. Stannek, A. Glinka, and C. Niehrs. 2005. Casein kinase 1 gamma couples Wnt receptor activation to cytoplasmic signal transduction. *Nature*. 438:867–872. http://dx.doi.org/10.1038/nature04170

Dietzl, G., D. Chen, F. Schnorrer, K.C. Su, Y. Barinova, M. Fellner, B. Gasser, K. Kinsey, S. Oppel, S. Scheiblauer, et al. 2007. A genome-wide transgenic RNAi library for conditional gene inactivation in *Drosophila*. *Nature*. 448:151–156. http://dx.doi.org/10.1038/nature05954

Dollar, G., E. Struckhoff, J. Michaud, and R.S. Cohen. 2002. Rab11 polarization of the *Drosophila* oocyte: a novel link between membrane trafficking, microtubule organization, and oskar mRNA localization and translation. *Development*. 129:517–526.

Eaton, S. 1997. Planar polarization of *Drosophila* and vertebrate epithelia. *Curr. Opin. Cell Biol.* 9:860–866. http://dx.doi.org/10.1016/S0955-0674(97)80089-0

Entchev, E.V., A. Schwabedissen, and M. González-Gaitán. 2000. Gradient formation of the TGF-beta homolog Dpp. *Cell*. 103:981–991. http://dx.doi.org/10.1016/S0092-8674(00)00200-2

Fletcher, S.J., and J.Z. Rappoport. 2009. The role of vesicle trafficking in epithelial cell motility. *Biochem. Soc. Trans.* 37:1072–1076. http://dx.doi.org/10.1042/BST0371072

Frescas, D., M. Mavrakis, H. Lorenz, R. Delotto, and J. Lippincott-Schwartz. 2006. The secretory membrane system in the *Drosophila* syncytial blastoderm embryo exists as functionally compartmentalized units around individual nuclei. *J. Cell Biol.* 173:219–230. http://dx.doi.org/10.1083/jcb.200601156

Fricke, R., C. Gohl, E. Dharmalingam, A. Grevelhörster, B. Zahedi, N. Harden, M. Kessels, B. Qualmann, and S. Bogdan. 2009. *Drosophila* Cip4/Toca-1 integrates membrane trafficking and actin dynamics through WASP and SCAR/WAVE. *Curr. Biol.* 19:1429–1437. http://dx.doi.org/10.1016/j.cub.2009.07.058

Gaengel, K., and M. Mlodzik. 2008. Microscopic analysis of the adult *Drosophila* retina using semithin plastic sections. *Methods Mol. Biol.* 420:277–287. http://dx.doi.org/10.1007/978-1-59745-583-1_17

Gray, R.S., P.B. Abitua, B.J. Wlodarczyk, H.L. Szabo-Rogers, O. Blanchard, I. Lee, G.S. Weiss, K.J. Liu, E.M. Marcotte, J.B. Wallingford, and R.H. Finnell. 2009. The planar cell polarity effector Fuz is essential for targeted membrane trafficking, ciliogenesis and mouse embryonic development. *Nat. Cell Biol.* 11:1225–1232. http://dx.doi.org/10.1038/ncb1966

Guichard, A., S.M. McGillivray, B. Cruz-Moreno, N.M. van Sorge, V. Nizet, and E. Bier. 2010. Anthrax toxins cooperatively inhibit endocytic recycling by the Rab11/Sec15 exocyst. *Nature*. 467:854–858. http://dx.doi.org/10.1038/nature09446

Hales, C.M., J.P. Vaerman, and J.R. Goldenring. 2002. Rab11 family interacting protein 2 associates with Myosin Vb and regulates plasma membrane

recycling. *J. Biol. Chem.* 277:50415–50421. http://dx.doi.org/10.1074/jbc.M209270200

Harumoto, T., M. Ito, Y. Shimada, T.J. Kobayashi, H.R. Ueda, B. Lu, and T. Uemura. 2010. Atypical cadherins Dachsous and Fat control dynamics of noncentrosomal microtubules in planar cell polarity. *Dev. Cell*. 19:389–401. http://dx.doi.org/10.1016/j.devcel.2010.08.004

Heasman, S.J., and A.J. Ridley. 2008. Mammalian Rho GTPases: new insights into their functions from in vivo studies. *Nat. Rev. Mol. Cell Biol.* 9:690–701. http://dx.doi.org/10.1038/nrm2476

Horgan, C.P., S.R. Hanscom, R.S. Jolly, C.E. Futter, and M.W. McCaffrey. 2010. Rab11-FIP3 links the Rab11 GTPase and cytoplasmic dynein to mediate transport to the endosomal-recycling compartment. *J. Cell Sci.* 123:181–191. http://dx.doi.org/10.1242/jcs.052670

Hummel, T., S. Attix, D. Gunning, and S.L. Zipursky. 2002. Temporal control of glial cell migration in the *Drosophila* eye requires gilgamesh, hedgehog, and eye specification genes. *Neuron*. 33:193–203. http://dx.doi.org/10.1016/S0896-6273(01)00581-5

Ito, N., and G.M. Rubin. 1999. gigas, a *Drosophila* homolog of tuberous sclerosis gene product-2, regulates the cell cycle. *Cell*. 96:529–539. http://dx.doi.org/10.1016/S0092-8674(00)80657-1

Jafar-Nejad, H., H.K. Andrews, M. Acar, V. Bayat, F. Wirtz-Peitz, S.Q. Mehta, J.A. Knoblich, and H.J. Bellen. 2005. Sec15, a component of the exocyst, promotes notch signaling during the asymmetric division of *Drosophila* sensory organ precursors. *Dev. Cell*. 9:351–363. http://dx.doi.org/10.1016/j.devcel.2005.06.010

Jenny, A., and M. Mlodzik. 2008. Modified vectors for the two-step directional cloning of inverted repeats for RNA interference in *Drosophila*. *Biotechniques*. 44:335–339. http://dx.doi.org/10.2144/000112720

Jenny, A., R.S. Darken, P.A. Wilson, and M. Mlodzik. 2003. Prickle and Strabismus form a functional complex to generate a correct axis during planar cell polarity signaling. *EMBO J.* 22:4409–4420. http://dx.doi.org/10.1093/emboj/cdg424

Jia, J., L. Zhang, Q. Zhang, C. Tong, B. Wang, F. Hou, K. Amanai, and J. Jiang. 2005. Phosphorylation by double-time/CKIepsilon and CKIalpha targets cubitus interruptus for Slimb/beta-TRCP-mediated proteolytic processing. *Dev. Cell*. 9:819–830. http://dx.doi.org/10.1016/j.devcel.2005.10.006

Jing, J., E. Tarbutton, G. Wilson, and R. Prekeris. 2009. Rab11-FIP3 is a Rab11-binding protein that regulates breast cancer cell motility by modulating the actin cytoskeleton. *Eur. J. Cell Biol.* 88:325–341. http://dx.doi.org/10.1016/j.ejcb.2009.02.186

Klein, T.J., and M. Mlodzik. 2005. Planar cell polarization: an emerging model points in the right direction. *Annu. Rev. Cell Dev. Biol.* 21:155–176. http://dx.doi.org/10.1146/annurev.cellbio.21.012704.132806

Krasnow, R.E., and P.N. Adler. 1994. A single frizzled protein has a dual function in tissue polarity. *Development*. 120:1883–1893.

Langevin, J., M.J. Morgan, J.B. Sibarita, S. Aresta, M. Murthy, T. Schwarz, J. Camonis, and Y. Bellaïche. 2005. *Drosophila* exocyst components Sec5, Sec6, and Sec15 regulate DE-Cadherin trafficking from recycling endosomes to the plasma membrane. *Dev. Cell*. 9:365–376. http://dx.doi.org/10.1016/j.devcel.2005.07.013

Lawrence, P.A., G. Struhl, and J. Casal. 2007. Planar cell polarity: one or two pathways? *Nat. Rev. Genet.* 8:555–563. http://dx.doi.org/10.1038/nrg2125

Lecuit, T. 2003. Regulation of membrane dynamics in developing epithelia. *Curr. Opin. Genet. Dev.* 13:351–357. http://dx.doi.org/10.1016/S0959-437X(03)00078-9

Lew, D.J., and S.I. Reed. 1995. Cell cycle control of morphogenesis in budding yeast. *Curr. Opin. Genet. Dev.* 5:17–23. http://dx.doi.org/10.1016/S0959-437X(95)90048-9

Li, B.X., A.K. Satoh, and D.F. Ready. 2007. Myosin V, Rab11, and dRip11 direct apical secretion and cellular morphogenesis in developing *Drosophila* photoreceptors. *J. Cell Biol.* 177:659–669. http://dx.doi.org/10.1083/jcb.200610157

Li, J., C. Yen, D. Liaw, K. Podsypanina, S. Bose, S.I. Wang, J. Puc, C. Miliaresis, L. Rodgers, R. McCombie, et al. 1997. PTEN, a putative protein tyrosine phosphatase gene mutated in human brain, breast, and prostate cancer. *Science*. 275:1943–1947. http://dx.doi.org/10.1126/science.275.5308.1943

Liu, S.L., N. Fewkes, D. Ricketson, R.R. Penkert, and K.E. Prehoda. 2008. Filament-dependent and -independent localization modes of *Drosophila* non-muscle myosin II. *J. Biol. Chem.* 283:380–387. http://dx.doi.org/10.1074/jbc.M703924200

Lloyd, T.E., R. Atkinson, M.N. Wu, Y. Zhou, G. Pennetta, and H.J. Bellen. 2002. Hrs regulates endosome membrane invagination and tyrosine kinase receptor signaling in *Drosophila*. *Cell*. 108:261–269. http://dx.doi.org/10.1016/S0092-8674(02)00611-6

Madden, K., and M. Snyder. 1998. Cell polarity and morphogenesis in budding yeast. *Annu. Rev. Microbiol.* 52:687–744. http://dx.doi.org/10.1146/annurev.micro.52.1.687

Mammoto, A., T. Ohtsuka, I. Hotta, T. Sasaki, and Y. Takai. 1999. Rab11BP/Rabphilin-11, a downstream target of rab11 small G protein implicated in vesicle recycling. *J. Biol. Chem.* 274:25517–25524. http://dx.doi.org/10.1074/jbc.274.36.25517

Marchal, C., R. Haguenauer-Tsapis, and D. Urban-Grimal. 2000. Casein kinase I-dependent phosphorylation within a PEST sequence and ubiquitination at nearby lysines signal endocytosis of yeast uracil permease. *J. Biol. Chem.* 275:23608–23614. http://dx.doi.org/10.1074/jbc.M001735200

Marco, E., R. Wedlich-Soldner, R. Li, S.J. Altschuler, and L.F. Wu. 2007. Endocytosis optimizes the dynamic localization of membrane proteins that regulate cortical polarity. *Cell*. 129:411–422. http://dx.doi.org/10.1016/j.cell.2007.02.043

Mellman, I., and W.J. Nelson. 2008. Coordinated protein sorting, targeting and distribution in polarized cells. *Nat. Rev. Mol. Cell Biol.* 9:833–845. http://dx.doi.org/10.1038/nrm2525

Mehta, S.Q., P.R. Hiesinger, S. Beronja, R.G. Zhai, K.L. Schulze, P. Verstreken, Y. Cao, Y. Zhou, U. Tepass, M.C. Crair, and H.J. Bellen. 2005. Mutations in *Drosophila* sec15 reveal a function in neuronal targeting for a subset of exocyst components. *Neuron*. 46:219–232. http://dx.doi.org/10.1016/j.neuron.2005.02.029

Morin, X., R. Daneman, M. Zavortink, and W. Chia. 2001. A protein trap strategy to detect GFP-tagged proteins expressed from their endogenous loci in *Drosophila*. *Proc. Natl. Acad. Sci. USA*. 98:15050–15055. http://dx.doi.org/10.1073/pnas.261408198

Mottola, G., A.K. Classen, M. González-Gaitán, S. Eaton, and M. Zerial. 2010. A novel function for the Rab5 effector Rabenosyn-5 in planar cell polarity. *Development*. 137:2353–2364. http://dx.doi.org/10.1242/dev.048413

Murthy, M., D. Garza, R.H. Scheller, and T.L. Schwarz. 2003. Mutations in the exocyst component Sec5 disrupt neuronal membrane traffic, but neurotransmitter release persists. *Neuron*. 37:433–447. http://dx.doi.org/10.1016/S0896-6273(03)00031-X

Nachury, M.V., A.V. Loktev, Q. Zhang, C.J. Westlake, J. Peränen, A. Merdes, D.C. Slusarski, R.H. Scheller, J.F. Bazan, V.C. Sheffield, and P.K. Jackson. 2007. A core complex of BBS proteins cooperates with the GTPase Rab8 to promote ciliary membrane biogenesis. *Cell*. 129:1201–1213. http://dx.doi.org/10.1016/j.cell.2007.03.053

Nerusheva, O.O., N.V. Dorogova, N.V. Gubanova, O.S. Yudina, and L.V. Omelyanchuk. 2009. A GFP trap study uncovers the functions of Gilgamesh protein kinase in *Drosophila melanogaster* spermatogenesis. *Cell Biol. Int.* 33:586–593. http://dx.doi.org/10.1016/j.cellbi.2009.02.009

Olguín, P., A. Glavic, and M. Mlodzik. 2011. Intertissue mechanical stress affects Frizzled-mediated planar cell polarity in the *Drosophila* notum epidermis. *Curr. Biol.* 21:236–242. http://dx.doi.org/10.1016/j.cub.2011.01.001

Otani, T., K. Oshima, S. Onishi, M. Takeda, K. Shinmyozu, S. Yonemura, and S. Hayashi. 2011. IKKε regulates cell elongation through recycling endosome shuttling. *Dev. Cell*. 20:219–232. http://dx.doi.org/10.1016/j.devcel.2011.02.001

Oztan, A., M. Silvis, O.A. Weisz, N.A. Bradbury, S.C. Hsu, J.R. Goldenring, C. Yeaman, and G. Apodaca. 2007. Exocyst requirement for endocytic traffic directed toward the apical and basolateral poles of polarized MDCK cells. *Mol. Biol. Cell*. 18:3978–3992. http://dx.doi.org/10.1091/mbc.E07-02-0097

Panek, H.R., J.D. Stepp, H.M. Engle, K.M. Marks, P.K. Tan, S.K. Lemmon, and L.C. Robinson. 1997. Suppressors of YCK-encoded yeast casein kinase 1 deficiency define the four subunits of a novel clathrin AP-like complex. *EMBO J.* 16:4194–4204. http://dx.doi.org/10.1093/emboj/16.14.4194

Park, W.J., J. Liu, and P.N. Adler. 1994. Frizzled gene expression and development of tissue polarity in the *Drosophila* wing. *Dev. Genet.* 15:383–389. http://dx.doi.org/10.1002/dvg.1020150410

Pataki, C., T. Matusek, E. Kurucz, I. Andó, A. Jenny, and J. Mihály. 2010. *Drosophila* Rab23 is involved in the regulation of the number and planar polarization of the adult cuticular hairs. *Genetics*. 184:1051–1065. http://dx.doi.org/10.1534/genetics.109.112060

Pelissier, A., J.P. Chauvin, and T. Lecuit. 2003. Trafficking through Rab11 endosomes is required for cellularization during *Drosophila* embryogenesis. *Curr. Biol.* 13:1848–1857. http://dx.doi.org/10.1016/j.cub.2003.10.023

Prekeris, R., J. Klumperman, and R.H. Scheller. 2000. A Rab11/Rip11 protein complex regulates apical membrane trafficking via recycling endosomes. *Mol. Cell*. 6:1437–1448. http://dx.doi.org/10.1016/S1097-2765(00)00140-4

Purvanov, V., A. Koval, and V.L. Katanaev. 2010. A direct and functional interaction between Go and Rab5 during G protein-coupled receptor signaling. *Sci. Signal.* 3:ra65. http://dx.doi.org/10.1126/scisignal.2000877

Rawls, A.S., and T. Wolff. 2003. Strabismus requires Flamingo and Prickle function to regulate tissue polarity in the *Drosophila* eye. *Development*. 130:1877–1887. http://dx.doi.org/10.1242/dev.00411

Riggs, B., W. Rothwell, S. Mische, G.R. Hickson, J. Matheson, T.S. Hays, G.W. Gould, and W. Sullivan. 2003. Actin cytoskeleton remodeling during early *Drosophila* furrow formation requires recycling endosomal components

Nuclear-fallout and Rab11. *J. Cell Biol.* 163:143–154. http://dx.doi.org/10.1083/jcb.200305115

Riggs, B., B. Fasulo, A. Royou, S. Mische, J. Cao, T.S. Hays, and W. Sullivan. 2007. The concentration of Nuf, a Rab11 effector, at the microtubule-organizing center is cell cycle regulated, dynein-dependent, and coincides with furrow formation. *Mol. Biol. Cell*. 18:3313–3322. http://dx.doi.org/10.1091/mbc.E07-02-0146

Robinson, L.C., M.M. Menold, S. Garrett, and M.R. Culbertson. 1993. Casein kinase I-like protein kinases encoded by YCK1 and YCK2 are required for yeast morphogenesis. *Mol. Cell. Biol.* 13:2870–2881.

Robinson, L.C., C. Bradley, J.D. Bryan, A. Jerome, Y. Kweon, and H.R. Panek. 1999. The Yck2 yeast casein kinase 1 isoform shows cell cycle-specific localization to sites of polarized growth and is required for proper septin organization. *Mol. Biol. Cell*. 10:1077–1092.

Ryder, E., M. Ashburner, R. Bautista-Llacer, J. Drummond, J. Webster, G. Johnson, T. Morley, Y.S. Chan, F. Blows, D. Coulson, et al. 2007. The DrosDel deletion collection: a *Drosophila* genomewide chromosomal deficiency resource. *Genetics*. 177:615–629. http://dx.doi.org/10.1534/genetics.107.076216

Salminen, A., and P.J. Novick. 1989. The Sec15 protein responds to the function of the GTP binding protein, Sec4, to control vesicular traffic in yeast. *J. Cell Biol.* 109:1023–1036. http://dx.doi.org/10.1083/jcb.109.3.1023

Satoh, A.K., J.E. O'Tousa, K. Ozaki, and D.F. Ready. 2005. Rab11 mediates post-Golgi trafficking of rhodopsin to the photosensitive apical membrane of *Drosophila* photoreceptors. *Development*. 132:1487–1497. http://dx.doi.org/10.1242/dev.01704

Shih, J., and R. Keller. 1992. Patterns of cell motility in the organizer and dorsal mesoderm of *Xenopus laevis*. *Development*. 116:915–930.

Shimada, Y., S. Yonemura, H. Ohkura, D. Strutt, and T. Uemura. 2006. Polarized transport of Frizzled along the planar microtubule arrays in *Drosophila* wing epithelium. *Dev. Cell*. 10:209–222. http://dx.doi.org/10.1016/j.devcel.2005.11.016

Sisson, J.C., C. Field, R. Ventura, A. Royou, and W. Sullivan. 2000. Lava lamp, a novel peripheral golgi protein, is required for *Drosophila melanogaster* cellularization. *J. Cell Biol.* 151:905–918. http://dx.doi.org/10.1083/jcb.151.4.905

Slaughter, B.D., A. Das, J.W. Schwartz, B. Rubinstein, and R. Li. 2009. Dual modes of cdc42 recycling fine-tune polarized morphogenesis. *Dev. Cell*. 17:823–835. http://dx.doi.org/10.1016/j.devcel.2009.10.022

Struhl, G., and K. Basler. 1993. Organizing activity of wingless protein in *Drosophila*. *Cell*. 72:527–540. http://dx.doi.org/10.1016/0092-8674(93)90072-X

Strutt, D.I. 2001. Asymmetric localization of frizzled and the establishment of cell polarity in the *Drosophila* wing. *Mol. Cell*. 7:367–375. http://dx.doi.org/10.1016/S1097-2765(01)00184-8

Strutt, D., and S.J. Warrington. 2008. Planar polarity genes in the *Drosophila* wing regulate the localisation of the FH3-domain protein Multiple Wing Hairs to control the site of hair production. *Development*. 135:3103–3111. http://dx.doi.org/10.1242/dev.025205

Strutt, D., R. Johnson, K. Cooper, and S. Bray. 2002. Asymmetric localization of frizzled and the determination of notch-dependent cell fate in the *Drosophila* eye. *Curr. Biol.* 12:813–824. http://dx.doi.org/10.1016/S0960-9822(02)00841-2

Strutt, H., and D. Strutt. 2008. Differential stability of flamingo protein complexes underlies the establishment of planar polarity. *Curr. Biol.* 18:1555–1564. http://dx.doi.org/10.1016/j.cub.2008.08.063

Strutt, H., and D. Strutt. 2009. Asymmetric localisation of planar polarity proteins: Mechanisms and consequences. *Semin. Cell Dev. Biol.* 20:957–963. http://dx.doi.org/10.1016/j.semcdb.2009.03.006

Tan, Y., D. Yu, J. Pletting, and R.L. Davis. 2010. Gilgamesh is required for rutabaga-independent olfactory learning in *Drosophila*. *Neuron*. 67:810–820. http://dx.doi.org/10.1016/j.neuron.2010.08.020

TerBush, D.R., T. Maurice, D. Roth, and P. Novick. 1996. The Exocyst is a multiprotein complex required for exocytosis in *Saccharomyces cerevisiae*. *EMBO J.* 15:6483–6494.

Turner, C.M., and P.N. Adler. 1998. Distinct roles for the actin and microtubule cytoskeletons in the morphogenesis of epidermal hairs during wing development in *Drosophila*. *Mech. Dev.* 70:181–192. http://dx.doi.org/10.1016/S0925-4773(97)00194-9

Ullrich, O., S. Reinsch, S. Urbé, M. Zerial, and R.G. Parton. 1996. Rab11 regulates recycling through the pericentriolar recycling endosome. *J. Cell Biol.* 135:913–924. http://dx.doi.org/10.1083/jcb.135.4.913

Vancura, A., A. Sessler, B. Leichus, and J. Kuret. 1994. A prenylation motif is required for plasma membrane localization and biochemical function of casein kinase I in budding yeast. *J. Biol. Chem.* 269:19271–19278.

Van Der Sluijs, P., M. Hull, A. Zahraoui, A. Tavitian, B. Goud, and I. Mellman. 1991. The small GTP-binding protein rab4 is associated with early endosomes. *Proc. Natl. Acad. Sci. USA*. 88:6313–6317. http://dx.doi.org/10.1073/pnas.88.14.6313

Wallingford, J.B., S.E. Fraser, and R.M. Harland. 2002. Convergent extension: the molecular control of polarized cell movement during embryonic development. *Dev. Cell*. 2:695–706. http://dx.doi.org/10.1016/S1534-5807(02)00197-1

Wang, P.C., A. Vancura, T.G. Mitcheson, and J. Kuret. 1992. Two genes in *Saccharomyces cerevisiae* encode a membrane-bound form of casein kinase-1. *Mol. Biol. Cell*. 3:275–286.

Wang, X., R. Kumar, J. Navarre, J.E. Casanova, and J.R. Goldenring. 2000. Regulation of vesicle trafficking in madin-darby canine kidney cells by Rab11a and Rab25. *J. Biol. Chem.* 275:29138–29146. http://dx.doi.org/10.1074/jbc.M004410200

Wang, Y., and J. Nathans. 2007. Tissue/planar cell polarity in vertebrates: new insights and new questions. *Development*. 134:647–658. http://dx.doi.org/10.1242/dev.02772

Winter, C.G., B. Wang, A. Ballew, A. Royou, R. Karess, J.D. Axelrod, and L. Luo. 2001. *Drosophila* Rho-associated kinase (Drok) links Frizzled-mediated planar cell polarity signaling to the actin cytoskeleton. *Cell*. 105:81–91. http://dx.doi.org/10.1016/S0092-8674(01)00298-7

Wong, L.L., and P.N. Adler. 1993. Tissue polarity genes of *Drosophila* regulate the subcellular location for prehair initiation in pupal wing cells. *J. Cell Biol.* 123:209–221. http://dx.doi.org/10.1083/jcb.123.1.209

Wu, H., G. Rossi, and P. Brennwald. 2008. The ghost in the machine: small GTPases as spatial regulators of exocytosis. *Trends Cell Biol.* 18:397–404. http://dx.doi.org/10.1016/j.tcb.2008.06.007

Wu, J., and M. Mlodzik. 2009. A quest for the mechanism regulating global planar cell polarity of tissues. *Trends Cell Biol.* 19:295–305. http://dx.doi.org/10.1016/j.tcb.2009.04.003

Wu, S., S.Q. Mehta, F. Pichaud, H.J. Bellen, and F.A. Quiocho. 2005. Sec15 interacts with Rab11 via a novel domain and affects Rab11 localization in vivo. *Nat. Struct. Mol. Biol.* 12:879–885. http://dx.doi.org/10.1038/nsmb987

Xu, T., and G.M. Rubin. 1993. Analysis of genetic mosaics in developing and adult *Drosophila* tissues. *Development*. 117:1223–1237.

Yan, J., D. Huen, T. Morely, G. Johnson, D. Gubb, J. Roote, and P.N. Adler. 2008. The multiple-wing-hairs gene encodes a novel GBD-FH3 domain-containing protein that functions both prior to and after wing hair initiation. *Genetics*. 180:219–228. http://dx.doi.org/10.1534/genetics.108.091314

Yoshimura, S., J. Egerer, E. Fuchs, A.K. Haas, and F.A. Barr. 2007. Functional dissection of Rab GTPases involved in primary cilium formation. *J. Cell Biol.* 178:363–369. http://dx.doi.org/10.1083/jcb.200703047

Zhang, J., K.L. Schulze, P.R. Hiesinger, K. Suyama, S. Wang, M. Fish, M. Acar, R.A. Hoskins, H.J. Bellen, and M.P. Scott. 2007. Thirty-one flavors of *Drosophila* rab proteins. *Genetics*. 176:1307–1322. http://dx.doi.org/10.1534/genetics.106.066761

Zhang, X.M., S. Ellis, A. Sriratana, C.A. Mitchell, and T. Rowe. 2004. Sec15 is an effector for the Rab11 GTPase in mammalian cells. *J. Biol. Chem.* 279:43027–43034. http://dx.doi.org/10.1074/jbc.M402264200

Zhou, F.Q., and C.S. Cohan. 2004. How actin filaments and microtubules steer growth cones to their targets. *J. Neurobiol.* 58:84–91. http://dx.doi.org/10.1002/neu.10278